submitted to *Geophys. J. Int.*

The fault slip budget in Guerrero, southern Mexico

Anthony R. Lowry,[1,2] Kristine M. Larson,[3] Vladimir Kostoglodov[4] and Osváldo Sanchez[4]

[1]*Department of Physics, University of Colorado, Boulder, Colorado, 80309-0390, U.S.A.*

E-mail: arlowry@himalaya.colorado.edu

[2]*Now at: Department of Geology, Utah State University, Logan, UT 84322-4505, U.S.A.*

[3]*Department of Aerospace Engineering Science, University of Colorado, Boulder, CO, 80309-0429, U.S.A.*

E-mail: Kristine.Larson@colorado.edu

[4]*Instituto de Geofísica, Universidad Nacional Autónoma de México (UNAM), Ciudad Universitaria, Del. Coyoacan C.P. 04510, México, D.F., México.*

E-mails: vladi@servidor.unam.mx; osvaldo@ollin.igeofcu.unam.mx

SUMMARY

GPS studies of Guerrero, southern Mexico, have described large slow slip events on the Cocos-North American plate boundary in 1996, 1998 and 2002. In this study, we show that five smaller events occurred in 1999, 2000, 2001, 2003 and 2004. These eight events are quasi-periodic with a period of 12.0$\pm$0.3 months, similar to periodic slow slip elsewhere but with more variable moment release. Perhaps the most important application of GPS data is to seismic hazard, but transient slip complicates estimation of the total strain moment available for seismic release. To examine seismic hazard in Guerrero, we model the slip deficit using two end-member representations of slow slip: (1) a single rectangular patch on the plate boundary, and (2) a 20-km-mesh discretization. The models yield very different estimates of slip location and moment release, but both models locate slow slip near the base of the seismogenic zone, and both require negligible slip during inter-event periods to surprising depth on the plate boundary. The discretized model con-

firms that slow slip can be driven by potential energy accumulated as slip deficit between events. Residual slip deficit accumulated during the 1992–2005 period of GPS observations, when extrapolated to the time since the last earthquake, is sufficient to generate a M_w=7.9–8.0 earthquake within the Guerrero gap segment of the subduction megathrust. We also find that, if oblique Cocos-North America motion is partitioned into upper-plate strike-slip faulting, all of the $\sim$8 mm yr^{-1} sinistral strike-slip is accommodated on the Atoyac and Chapala-Oaxaca fault zones.

Key words: slow slip events – seismotectonics – seismic hazard – fault friction

1 INTRODUCTION

Subduction margins exhibit a rich variety of transient aseismic fault slip, including postseismic slip following large megathrust earthquakes (Kawasaki et al. 1995; Heki et al. 1997; Bürgmann et al. 2001; Hutton et al. 2001), preslip preceding great earthquakes (Linde & Silver 1989; Gordeev et al. 2001), and slip events that occur without obvious space-time relation to large earthquakes. The latter, referred to as "slow slip events" or "silent earthquakes", have been documented in New Zealand (Douglas et al. 2005), Japan (Hirose et al. 1999; Ozawa et al. 2001; Obara et al. 2004), Alaska (Freymueller et al. 2003), Cascadia (Dragert et al. 2001; Miller et al. 2002), Mexico (Lowry et al. 2001; Kostoglodov et al. 2003; Larson et al. 2004) and Costa Rica (Protti et al. 2005). These locations correspond to virtually every subduction margin on the Pacific rim with more than five years of continuous GPS (CGPS) network observations.

Most studies of slow slip events to date focus on observational aspects of the phenomenon such as the timing and amount of measured displacement or tilt, and relationships to timing and location of the harmonic tremor that commonly accompanies slow slip (e.g., Rogers & Dragert 2003; Obara et al. 2004; Szeliga et al. 2004). Some studies take the additional step of modeling the geodetic data to characterize moment release and location of slip on the plate interface (e.g. Ozawa et al. 2001; Larson et al. 2004; Melbourne et al. 2005). However, there is also a broadly-recognized need for inquiry that addresses (1) the physical process or mechanism of slip and (2) the implications of slip for timing and magnitude of future great earthquakes.

Several mechanisms for slow slip have been hypothesized. Coincidence of slow slip and harmonic tremor has led some to suggest that slow slip is driven by dewatering events on the subducting slab that temporarily decrease fault frictional resistance (Julian 2002; Melbourne & Webb 2003). Alternatively, modeling of rate-state frictional slip has shown that slip events arise spontaneously given minor

variations in fault frictional properties and a transient background stress process (Liu & Rice 2005). Periodicity of events in Cascadia and elsewhere has also led to the suggestion that slow slip is forced or modulated by the pole-tide (Shen et al. 2005) or other environmental stress (Lowry 2006). Distinguishing between these and other possible mechanisms will require careful attention to the observational constraints, and knowledge of their limitations.

The question of what slow slip implies for future great earthquakes has two components. One relates to whether slow slip provides clues as to the timing of the next great earthquake on the subduction megathrust. Various researchers have suggested that slow slip adds incrementally to the Coulomb failure state within the area of future great earthquakes (Hirose et al. 1999; Thatcher 2001), and Liu & Rice (2005) found that in some instances slow slip events modeled via rate-state-frictional dynamics propagate updip into the seismogenic zone where they can accelerate to earthquake rupture speeds. A second, more fundamental question is whether slow slip increases the earthquake potential within the seismogenic zone (by increasing stress) or decreases it (by relieving strain energy). This translates to a question of where precisely slip is occurring, which is difficult to determine from GPS data because estimates are highly sensitive to poorly-determined vertical displacement. Most modeling has suggested that slow slip occurs at, or just downdip of, the base of the seismogenic zone (e.g., Dragert et al. 2001; Melbourne et al. 2005). If that location estimate is correct, Coulomb stress within the seismogenic zone is increased, the fault moves closer to failure, and the integral of seismogenic zone slip deficit (i.e., strain energy available for earthquake release) is unchanged by slow slip. Alternatively, some have suggested that slow slip occurs within the seismogenic zone (e.g., Kostoglodov et al. 2003; Douglas et al. 2005), in which case it may actually reduce seismic hazard. On the Cocos-North American subduction boundary in southern Mexico, some researchers even suggest that the Guerrero seismic gap is a gap because virtually all interplate strain is released in slow slip events (e.g., DeMets et al. 2004).

The latter question, i.e., whether slow slip events may significantly reduce earthquake potential, is the topic of this paper. Here we examine the earthquake potential of the Guerrero seismic gap, where slow slip has been hypothesized to delay or prevent great earthquakes. Several million people live within the seismic radiation near-field expected for a Guerrero gap earthquake, and Guerrero is also the nearest plate boundary segment to Mexico City (population $>$17 million) where basin amplification of waves from a 1985 M_w=8.1 earthquake on a more distant segment of the plate boundary killed up to 10,000 people and caused billions of dollars in structural damage. Hence, resolving the question of how slow slip affects seismogenesis there has potentially far-reaching societal implications.

Estimating seismic potential (i.e., the integral of slip deficit within the seismogenic zone) is greatly complicated if a substantial fraction of slip occurs in slow slip events. Fully addressing the seismic

potential requires (1) a modeling approach that quantifies the entire slip budget (including all slow slip events plus the accumulation of slip deficit during interevent periods) and (2) careful attention to the range of uncertainty in estimates of slip deficit. To our knowledge, an analysis of this type has not previously been attempted anywhere in the world. As part of our analysis, we demonstrate that five small slow slip events are evident in the Guerrero GPS data that have not been described in previous publications. We also examine the question of which upper-plate structures may accommodate oblique motion of the Cocos plate relative North America, with attendant implications for other sources of seismic hazard in southern Mexico.

2 GUERRERO SEISMOTECTONICS

Neotectonics and seismic hazard of southern Mexico are dominated by Cocos-North America plate boundary deformation (Figure 1). Cocos oceanic lithosphere subducts beneath North America at the Middle America trench, $\sim$60 to 80 km south of the southern coast of Mexico. NUVEL1-A (DeMets et al. 1994) convergence rates increase eastward along the plate boundary from 4.7 cm/yr near Colima to 6.5 cm/yr in Chiapas. Relative motion is slightly ($\sim$12°) oblique to the trench normal, yielding a sinistral component of $\sim$1 cm/yr. The plate interface beneath Guerrero has an unusual "flat slab" geometry (Suárez et al. 1990; Pardo & Suárez 1995; Kostoglodov et al. 1996) with a shallow dip ($\sim$7–12°) between the trench and the coastline, steepening to 20–30° between the coast and about 50 km inland, and flattening (dip $\sim 5°$) from there to the volcanic arc about 200 km further inland.

Rapid Cocos-North American convergence generates major earthquakes on the shallow subduction megathrust at 30–100 year intervals (Kostoglodov & Ponce 1994). However, two segments of the plate boundary– one in the Gulf of Tehuantepec, the other in central Guerrero state– have not ruptured since 1923, when the first Mexican seismograph network was installed. A third "seismic gap" was filled by the M_w=7.6 Colima earthquake in January of 2003 (Figure 1). The Guerrero seismic gap may correspond to the rupture area of a December 16, 1911 (M_s=7.8) event (Figure 1 inset), although seismic data from the time are inadequate to establish the mechanism and hypocentral location. Since 1911, the region has experienced more than 5 m of relative plate motion.

Within the continental interior, major fault structures such as the Chapala-Oaxaca fault zone, the Atoyac fault and the Chapala-Tula fault zone (CTFZ) accommodate poorly-known internal deformation of the North American upper plate (e.g., Johnson & Harrison 1990). Extension plus some additional component of sinistral strike-slip occurs across CTFZ structures in the Trans-Mexican volcanic belt (Figure 1). Based on slip lineations, fault offsets and cross-cutting relations, Suter et al. (2001) estimate extension across the CTFZ at 0.2$\pm$0.05 mm yr^{-1}, with a smaller component of sinistral strike-slip on short, discontiguous faults. Paleomagnetic studies (e.g., Ruiz-Martínez et al. 2000)

similarly indicate post-Miocene strain across the CTFZ to be extensional with a minor sinistral component. Regional-scale GPS velocities alternatively permit up to 4 mm yr^{-1} of sinistral strike-slip motion across the CTFZ (Márquez-Azúa & DeMets 2003). The Chapala-Oaxaca and Atoyac faults are known almost exclusively from thematic mapping, and so their slip rates are unconstrained. The risk of a large, near-term earthquake is less on these upper-plate faults than on the coastal megathrust. Nevertheless, it is important to characterize also the seismic potential of upper-plate structures because they are shallower and more proximal to several major Mexican population centers.

3 DEFORMATION MEASUREMENTS

A twenty-one site GPS campaign network was initially measured in Guerrero in 1992 (Figure 2). Four sites were resurveyed following the September 14, 1995 Copala earthquake, and twelve coastal sites were resurveyed in April 1996. In November 1998, eight sites were reoccupied and an additional ten sites were installed and measured. All of the 1998 network sites and fifteen of the original 1992 sites were resurveyed in October 2000. Smaller surveys were conducted in October and November 2001, and May to November 2002. Larson et al. (2004) gives a more detailed description of campaign measurements.

The first CGPS site in Guerrero was established at CAYA in January, 1997. CGPS instruments were installed at ZIHP, ACAP, and IGUA in summer-fall 2000, and at DOAR and COYU in spring of 2003. Sites were installed in neighboring Oaxaca state in July 2000 (PINO) and February 2001 (OAXA). This study also uses data from a GPS receiver installed to study volcano deformation at Popocatépetl (POSW) in March of 1996 and another receiver (YAIG) installed in February 1999; both of these are in the state of Morelos just northeast of Guerrero.

GPS data are analyzed with the GIPSY-OASIS software package (Lichten & Border 1987). Orbits generated by the Jet Propulsion Laboratory are used to estimate coordinates in the ITRF2000 reference frame (Zumberge et al. 1997; Altamimi et al. 2002). In the weighted least squares analysis of GPS observations, receiver coordinates, receiver clock behavior, and zenith tropospheric delays are estimated via standard strategies (Larson et al. 2004). Carrier phase ambiguities are resolved (Blewitt 1989) at a high percentage of sites for all surveys except during 1992. CGPS sites at McDonald Observatory, Texas (MDO1), Table Mountain, Colorado (TMGO), and Pie Town, New Mexico (PIE1) are included in the network solutions to tie the Guerrero network to sites on the stable North American plate. These sites were not installed until the mid-1990's, so 1992 solutions include only the local sites. GPS coordinates used in this analysis are baseline measurements relative to either MDO1 or ACAP (the latter only in the case of early campaign data). The baseline solutions minimize common-mode errors due to e.g. orbit errors and seasonal loading signals.

4 IDENTIFYING SLOW SLIP EVENTS

Identifying likely slow slip events in the GPS data is a necessary first step in characterizing the slip budget (and hence the seismic potential) of a subduction megathrust. In Guerrero, previous studies have examined events in 1995–1996 (Larson et al. 2004), 1998 (Lowry et al. 2001; Larson et al. 2004) and 2002 (Kostoglodov et al. 2003; Yoshioka et al. 2004; Iglesias et al. 2004). DeMets et al. (2004) suggest, based largely on proprietary INEGI data, that smaller events may have occurred in 1999, 2000 and 2001. Here we use a deformation modeling tool that fits a hyperbolic tangent function (HTF) to the GPS data to evaluate whether there is indeed evidence for smaller slip events in addition to the large, well-studied 1996, 1998 and 2002 slip.

4.1 HTF Analysis

Anomalous displacements during slow slip events can be estimated by fitting the GPS coordinate time series with a function of the form:

$$\vec{x}(t) = \vec{x}_0 + \vec{V}t + \sum_{i=1}^{n} \frac{\vec{U}_i}{2} \left[\tanh\left(\frac{t - T_{0i}}{\tau_i} \right) - 1 \right] \quad (1)$$

in which $\vec{x}(t)$ are GPS site coordinates at time t, $\vec{x}_0$ are coordinates at a reference time, $\vec{V}$ is a background or "steady-state" velocity, $\vec{U}_i$ is anomalous displacement during the i^{th} of n slow slip events, T_{0i} is the median time of the i^{th} event, and τ scales the period over which the event occurred. If T_0 and τ are specified, the other parameters can be estimated from linear least-squares inversion. We have developed an algorithm for grid search over T_0 and gradient search over τ to estimate anomalous deformation during slow slip events (http://anquetil.colorado.edu/∼arlowry/code_release.html). Linear parameters of velocity and transient displacement are estimated via least squares minimization, weighted by the formal inverse variance of GPS coordinate estimates. Formal parameter uncertainties of velocity and displacement are then scaled to yield a reduced χ^2 parameter of one.

HTF analysis using equation 1 can be used as a tool to distinguish probable slow slip events from correlated errors (e.g., monument wander and GPS position errors) or non-tectonic deformation that might otherwise be mistaken for slow slip. In our initial analyses, we require that the following criteria be met before examining whether a coordinate anomaly might indicate a slow slip event: (1) HTF modeling must minimize misfit at several different sites at approximately the same (independently determined) midtime T_0. (2) Total displacement at these sites must significantly exceed the 95% confidence interval of the displacement estimate. (3) The largest displacements should occur near the coast (as observed in the largest events), and all sites should move predominantly toward the trench (as expected for thrust slip on the plate boundary). Once each of these criteria have been established for a given time series anomaly, additional analyses can be performed to rule out alternative interpretations.

In Table 1, we list displacements resulting from HTF modeling of all time series anomalies that meet the above criteria. We include only those displacements that can be separated reliably from displacement in other likely events and from the estimate of background velocity (i.e., displacements at CGPS sites with measurements bracketing a given event). Displacement estimates adopt a timescale τ=1.8 months (which minimized the misfit for uniform τ). In some cases temporal sampling was insufficient to determine a midtime T_0; in those instances (denoted by approximate times in Table 1) we use the average T_0 at other sites to estimate displacements. North components of best fit functions from this analysis are shown as dashed lines in Figure 2. Figure 3 shows the vertical and trenchward horizontal components of displacements listed in Table 1, for each coordinate anomaly that met the criteria for a possible slip event. In each event, most of the sites move toward the trench. The exceptions (most often, inland sites IGUA, POSW, and YAIG) have zero trenchward motion within uncertainties except in 2001, when both IGUA and POSW move significantly away from the trench. Also, in each event most sites move upward. Generally the exceptions are, again, inland sites (IGUA, OAXA, POSW and YAIG) with motion near zero or downward.

Time-dependence of coordinate anomalies is similar for all events. If timescales are allowed to vary, all well-sampled time series are best-fit by τ between 1.6 and 2.5 months. The best-fit mid-time T_0 of transient deformation tends to occur earlier at the coastal sites and later at inland sites (Table 1), but is otherwise similar at all sites in a given year. The patterns of behavior are consistent across all events, and so it is reasonable to infer that if the largest ($\sim$10 cm in 2002) displacements result from slow slip, then smaller displacements also represent slow slip. It is also worth noting that in each possible event described here, most if not all sites move further toward the trench than the maximum horizontal motion (about 6 mm) observed in Cascadia slow slip events (Melbourne et al. 2005).

4.2 Annual Recurrence of Events

Other features of the potential slow slip events are intriguing, and not least among those is the recurrence behavior. Since Guerrero CGPS measurement began, events occur about once per year and always within $\pm$1.5 months of the mean T_0 $\sim$February 15. If one more rigorously regresses the time interval between events versus the number of intervening events for all permutations of event pairs from 1998 to 2004, the recurrence interval for events is 12.0$\pm$0.3 months– i.e., events are quasi-periodic with period almost exactly one year. This behavior mirrors quasi-periodicity of slow slip observed, e.g., in various different parts of the Cascadia subduction zone (Miller et al. 2002; Szeliga et al. 2004; Malone et al. 2004) and in southwest Japan (Obara et al. 2004). Periods at these other locations range from 10.9 to 13.9 months, and displacement time series are qualitatively similar to Guerrero behav-

ior except that trenchward displacements in Guerrero events are much more variable than observed elsewhere.

If Guerrero events are quasi-periodic with annual period, one would expect that a slow slip event should have occurred in late 1996 or early 1997 as well. Unfortunately, CAYA did not begin measurement until January of 1997 and shows no unequivocal evidence of an anomaly in its earliest coordinates. POSW was operating continuously at the time and does exhibit anomalous motion (Figure 2), but the direction is opposite that expected for slow slip and the timing correlates with eruptive activity of Popocatépetl volcano on which it sits (Larson et al. 2004). POSW motions are negligibly small during the 1999, 2000 and 2001 events, and smaller CAYA motions are recognizable only with ample measurement before and after, so we cannot rule out the possibility of a small slow slip event in 1997. Nevertheless GPS measurements at that time do not meet our criteria for identifying possible slip. One could argue that the 1996 event does not meet our criteria either, because motion is observed at only one station (ACAP) in the analysis presented here. However we include it because campaign GPS measurements show even larger trenchward displacements at three other sites (Larson et al. 2004).

4.3 Alternative Interpretations to Slow Slip

Some researchers might understandably be uncomfortable with the prospect of slow slip events having a recurrence interval of exactly one year. Virtually all CGPS coordinate time series contain annual signals (e.g., Blewitt & Lavallée 2002; Nikolaidis 2002), comprised of a variety of signals including elastic deformation by annual changes in surface mass loading, poroelastic deformation by groundwater changes, annual terms in atmospheric modeling error, and orbital mismodeling deriving from the other three. Hence, some might infer (at least in the case of the smaller events) that the apparent annual periodicity actually represents other signals that somehow mimic slow slip events. We consider each of these possible signal sources in turn.

At annual periods, surface mass loading in North America is dominated by continental hydrology with much smaller (order 10%) contributions from ocean bottom pressure and the atmosphere (Wahr et al. 1998). Here we focus our attention on the dominant load deformation by continental hydrologic mass. Our model of load deformation is forced by the global hydrologic mass model of Fan & van den Dool (2004), and we use continental PREM elastic and density parameters (Dziewonski & Anderson 1981) modified by CRUST2.0 parameters (Bassin et al. 2000) specific to each of the CGPS sites. Three-dimensional surface displacements are calculated at each CGPS site and differenced to those at MDO1. The deformation time series was resampled at the temporal sampling of each GPS site, and HTF analysis was performed using the same parameters T_0 and τ=1.8 months estimated from the CGPS measurements. Resulting estimates of displacement are shown as light grey circles in each panel

of Figure 3 for comparison. In contrast to the observed displacements, elastic load deformation affects predominantly the vertical component and has negligible horizontal expression. The only similarity to the GPS observations is that coastal sites tend to have relatively large ($\sim$10 mm) upward vertical displacements, whereas inland sites tend to move downward or not at all.

If we further allow timing parameters T_0 and τ to vary in HTF analyses of the simulated load deformation, we find the average optimal mid-time of elastic loading occurs about 1.1 months earlier than the mid-time derived from GPS observations, and the timing of deformation is much less variable ($\pm$0.3 months for elastic load response versus $\pm$1.5 months for timing of the observed events). Also, whereas events observed at inland sites consistently occur later than at coastal sites in the CGPS data, the timing of elastic load deformation is identical everywhere. Most telling, the optimal timescale τ of the simulated elastic loading signal is a very consistent 3.0 to 3.5 months (with mean 3.2), nearly twice the τ=1.6 to 2.5 months (mean 1.8) derived from GPS measurements. Hence the timescale of the measured events is far shorter than would be expected for a phenomenon (like hydrologic loading) with an approximately sinusoidal annual expression.

Our simulated loading signals are subject to errors including uncertainties in Earth elastic parameters and uncertainties in the weather models from which the hydrologic loading fields were derived. Variations in crustal properties perturb load response by less than 50% relative to the PREM continental average (Lowry et al. 2006). We have corrected for those variations here, so elastic parameterization error is unlikely to exceed 10–20%. Errors associated with Fan & van den Dool's (2004) hydrologic mass fields are liable to be a similarly small percentage of total displacement in southern North America, where snow loading effects are negligible. Despite uncertainties, it is clear that elastic loading cannot generate horizontal displacements observed in the GPS data, and moreover has a very different time-dependence.

Other CGPS signal sources can generate significant horizontal motions with annual period. Poroelastic deformation associated with groundwater storage and withdrawal observed in the Los Angeles basin, for example, exceeds several cm of horizontal motion (Bawden et al. 2001). However these are very localized (i.e., basin-specific) effects that could not generate displacements with consistent horizontal direction across scales of hundreds of km. Similarly, annual terms in atmospheric modeling error should be location-specific. Orbital error is mostly removed in this study by baseline differencing, but remainder terms should not vary significantly on the scale of the Guerrero network. Hence, the most reasonable explanation for both large and small displacement events observed in the GPS data is slow slip on the plate interface.

5 MODELING PLATE BOUNDARY SLIP

Modeling of slow slip events is ambiguous for several reasons, including (1) small signal-to-noise ratios (SNR) of GPS measurements (particularly in the vertical, which is needed to locate slip), and (2) spatial aliasing of surface deformation (e.g., Melbourne et al. 2005). In Guerrero, SNR of the largest events is the highest yet observed because the displacements are so large. However, SNR of the smaller events is no better than (and in some cases worse than) that of slow slip in Cascadia, and spatial sampling (especially for early events) is extremely sparse.

Nevertheless, modeling is a necessary step on the path to characterizing seismic potential in Guerrero. To address the issue of potential model ambiguity/error, we examine slip using two very different modeling approaches chosen expressly to represent "end-member" cases of slip inversion. Both approaches model time series of the GPS data by assuming constant steady-state slip during inter-event periods and time-variable slip during slip events. We invert all three components of the time series of GPS position data. Prior to modeling, coordinates are corrected for secular bias resulting from rigid plate motion. Analyses in §4.3 suggest that hydrologic loading can bias estimates of event vertical displacement by up to 1.6 cm, so we also subtract load deformation modeled in §4.3 from the time series at each site prior to slip modeling.

In both modeling approaches used here, GPS site coordinates $\vec{x}(t)$ are modeled using

$$\vec{x}(t) = \vec{x}_0 + \vec{V}t + \oint \vec{S}\left(\vec{\zeta}, t\right) G\left(\vec{x}, \vec{\zeta}\right) \mathrm{d}\vec{\zeta}. \tag{2}$$

Here, $\vec{V}$ is constant velocity at the GPS site from a steady-state virtual slip model (e.g., Savage 1983), $\vec{\zeta}$ denotes location on the fault surface, G is the deformation Green's function (Okada 1985), and $\vec{S}$ is a functional describing the transient component of slip. $\vec{S}$ is parameterized as having time dependence described by

$$\vec{S}(t) = \frac{\vec{S}_0}{2}\left[\tanh\left(\frac{t - T_0}{\tau}\right) - 1\right] \tag{3}$$

in which $\vec{S}_0$ is the total slow slip at a given location during a given event.

The approach to modeling steady-state slip is the same in both models. Slip on a surface approximating the megathrust geometry is discretized at a 20 km scale within the region of Guerrero network coverage and more coarsely outside that area. We assume that steady-state slip is some fraction of the relative plate motion, $\vec{\Phi} = (\vec{S}_{\mathrm{rpm}} + \vec{S}_b)/\vec{S}_{\mathrm{rpm}}$. Here, $\vec{S}_{\mathrm{rpm}}$ is slip at the relative plate motion rate and $\vec{S}_b$ is the back-slip rate (e.g., Savage 1983). The direction and rate of Cocos-North America relative plate motion varies significantly within the study region, so relative plate motion is approximated as constant within segments and equal to the NUVEL-1A model prediction at the center of the segment. We solve separately for fractional strike-slip Φ^{ss} and fractional dip-slip Φ^{ds}. The solution space is

restricted by imposing constraints that (1) $0 \leq \vec{\Phi} \leq 1$, (2) $\Phi^{ss} \leq \Phi^{ds}$, and (3) $\vec{\Phi}$ on neighboring segments cannot differ by more than 0.5, thus smoothing the discretized slip (Larson et al. 2004). Site velocity response is calculated for the no-slip condition ($\vec{\Phi} = \vec{0}$) on each segment. We then solve for the model parameters $\vec{\Phi}$ that minimize differences between the modeled and "observed" steady-state components of GPS velocity, subject to the constraints. Here, the "observed" steady-state velocity is estimated from residual GPS time series after subtracting a best-fit model (as described below) of the displacements at a given site during each of the eight slow slip events and the 1995 Copala earthquake.

5.1 Model I: Slip in a Rectangular Patch

The first approach to modeling slow slip consists of a weighted least-squares inversion for eight parameters of anomalous slip in a single rectangular patch. The parameters include timing parameters T_0 and τ, the along-strike length L and downdip width W of the slip patch, the center location (X_0, Y_0) of the patch, and the strike-slip and dip-slip components of total slip S_0^{ss} and S_0^{ds}. A more detailed description of this modeling approach is given in Larson et al. (2004), which uses a similar inversion except that the time series of GPS data modeled in that paper ended in 2001.75 and the modeling assumed that only two transients had occurred during the measurement interval (in 1996 and 1998). Here, we additionally invert for one slip patch each to represent the 1999, 2000, 2001, 2003 and 2004 events, and we also invert for two rectangular slip patches to represent the 2002 event described by Kostoglodov et al. (2003). Representing slip by a rectangular patch has the disadvantage that, if (as is most probably always the case) slip is highly spatially variable, the solution will be overdamped and consequently biased. However, because the number of model parameters is small, we can calculate parameter uncertainties.

5.2 Model II: Discretized Slip

For the second modeling approach, we first estimate displacement at each site during a given event by fitting equation (1) to the GPS time series, and then we use those displacements to invert for total anomalous slip $\vec{S}_0$ on the same gridded plate interface as was used for the steady-state model. We invert for strike-slip and dip-slip components subject to the constraint that slip in each patch cannot exceed the slip deficit accumulated since the beginning of GPS observation in 1992.25, i.e., $\vec{S}_{0i} \leq (T_{0i} - 1992.25)\vec{\Phi}\vec{V}_{\rm rpm} - \sum_{j=1}^{i-1} \vec{S}_{0j}$. This constraint serves the dual purpose of limiting the solution space and testing the physical expectation that slow slip events release elastic strain potential energy accumulated by frictional coupling on the fault. A second constraint forces the fractional strike-slip during a given event not to exceed the fractional dip-slip, i.e., $S_0^{ss}/V_{\rm rpm}^{ss} \leq S_0^{ds}/V_{\rm rpm}^{ds}$.

5.3 Model Results

Example best-fit models of slip during the 2002, 2003 and 2004 slow slip events are depicted in Figures 4–6. In each figure, the upper panel (part a) represents the best-fit rectangular patch model, and the lower panel (part b) depicts the best-fit discretized model, as described in §5.1 and §5.2 respectively. These can be thought of as representative of a large, intermediate and small Guerrero event respectively. Because these are the most recent of the events examined here, they are also the best sampled by GPS measurement.

The best-fit for each of the patch models is depicted by a rectangle, but we also show the range of possible solutions at 95% confidence. The grid search for best-fit patches entails hundreds of thousands of models of each event during each iteration, and each of those individual models is assigned a confidence using the likelihood ratio method of Beck & Arnold (1977). We have plotted (in grayscale contour) the minimum parameter confidence of all models that slipped at a given location and still fit the data at less than 95% confidence. Blank areas on the map correspond to regions where slip models could not fit the data at 95% confidence. Larger events are generally better constrained than smaller events, and later events are better-constrained than earlier events which rely heavily on campaign GPS measurements.

The centroid location of slip in the discretized models differs significantly from that in the patch models. During smaller events, discretized model slip is small (maximum 4 to 8 cm) and focuses near the coastline (i.e., within and near the base of the seismogenic zone as approximated from great earthquake rupture zones and aftershock distributions on segments neighboring the Guerrero gap). During larger events, slow slip has contributions from the same region of the seismogenic zone activated in smaller events plus larger (maximum 10 to 25 cm) slip contributions from deeper regions (to as much as 50 km downdip of the base of seismogenesis). Patch model slip, by contrast, occurs almost entirely downdip of the base of the seismogenic zone in all events, so the models are most similar during the largest events such as 2002 (Figure 4). Moreover, most of the slip in the discretized models occurs outside the 95% confidence range for location of “well-constrained” patch models. The difference in model estimates of slip location is most apparent in cumulative slip from all events (Figure 7). The amount of slip estimated by the two methods is also quite different. Where rectangular patch models congregate, total slow slip significantly exceeds the $\sim$0.8 m relative plate motion during the 1992–2005 period of GPS observations. The discretized model slip is 30 cm or less throughout the plate boundary. Correspondingly, the equivalent moment magnitude of strain release during each event differs significantly for the rectangular patch versus discretized models (Table 2). Moment release estimated for the discretized models is generally smaller than for rectangular patch models, and

in many cases (e.g., the 2002 event) the discretized model moment release is much less than the 95% confidence range estimated for the patch model.

Solutions for steady-state slip are shown in Figure 8. Velocities calculated from residuals of the transient models agree reasonably well with the best-fit models of steady-state slip in both cases, but the "observed" velocities are very different for the two models because the transient displacement models subtracted prior to estimating velocity are different. Nevertheless, both models indicate substantial coupling of the plate interface to a distance of about 200 km from the trench (corresponding to depths of $\sim$45–50 km). The limit of coupling is about 100 km further from the trench, and 20 km deeper, than the downdip limit of seismogenesis in megathrust earthquakes. Also, both models suggest higher slip rates in the lower portion of the seismogenic zone than at greater depths, below the frictional transition. The model which represents slow slip events as rectangular patches (Figure 8a) implies the shallow plate boundary is less strongly coupled than does the model with discretized slow slip. This is because the patch model forces all slow slip to occur on deeper portions of the plate boundary, so any shallow thrust slip needed to reconcile total deformation with the relative plate motion must be absorbed into the model of steady-state slip. The discretized model partitions more of the shallow thrust slip into the slow slip events.

Both the rectangular patch and discretized models yield good fits to the GPS time series. Some example time series are shown in Figure 9. The weighted (by inverse variance of the coordinate error) root-mean square (WRMS) of the model misfit for all 35 GPS sites is 5.03 mm for the best-fit rectangular patch model and 4.84 mm for the discretized model. The significantly smaller misfit of the discretized slow slip model is consistent with the much greater number of model parameters. In general, best-fit model predictions of transient displacement compare favorably with measurements from fitting equation (1) to the GPS time series (Figures 4–6). Modeled and estimated vectors of transient displacement are generally more similar in the case of the discretized slip model. An important component of this model is the correction for load deformation using simulated elastic response to a model of hydrologic loading, as described in §4.3. We evaluate the correction for load deformation by running the discretized model inversion both with and without the correction. The best-fit model without correction has WRMS misfit 4.87 mm, while the WRMS of the correction is 0.55 mm. If the 4.84 mm corrected misfit and the correction itself are treated as white noise processes, their RMS sum would predict a 4.87 mm misfit, suggesting that our simulated correction is a good approximation of the true load deformation. However, load deformation behaves more like correlated rather than white noise. Consequently if the best-fit model of the uncorrected time series is compared with a corrected time series, misfit is 4.89 mm, confirming that uncorrected load deformation tends to bias model estimates of the slow slip.

6 DISCUSSION

Although the primary objective of this analysis is to evaluate seismogenic potential of the Guerrero plate boundary, model results presented in §5.3 have implications for several other aspects of slow slip in subduction zones. These include implications for the physical processes that drive slow slip and for observations derived from slip modeling, both in Guerrero and elsewhere.

6.1 General Implications for Modeling Slow Slip

Discrepancies in location and moment release of the patch and discretized models relate to nonuniqueness of solutions for slip from the surface displacement data, and the differences in solution damping imposed by the models. These discrepancies are exacerbated by the sparse distribution of GPS observations in Guerrero, but low SNR of GPS data (particularly in the vertical) and measurement sampling that aliases potential source locations are ubiquitous in GPS network observations of slow slip. Consequently, these models would undoubtedly exhibit similar differences if they were applied to slow slip elsewhere, including if they were applied to events with better spatial sampling. All modeling of slow slip falls somewhere on the spectrum between the rectangular patch model and the discretized model presented here, and so effects of model parameterization should be considered when interpreting model-derived observations of slow slip. Numerous studies examine location and moment release of slow fault slip using either the discretized (e.g., Ozawa et al. 2001, 2004; Miyazaki et al. 2003) or patch (e.g., Hirose et al. 1999; Obara et al. 2004; Hirose & Obara 2005) modeling approaches. In Guerrero, the 2002 slip event has been ascribed a moment magnitude of 6.8 by a 20 km mesh discretized model and 7.5 by a patch model (this study), $\sim$7.5 from a two-dimensional forward model (Kostoglodov et al. 2003), 7.4 on fault discretizations of 30 to 100 km mesh using a Bayesian approach (Yoshioka et al. 2004), and 7.6 on a 50–100 km mesh discretization model (Iglesias et al. 2004). Our results indicate that caution is warranted when comparing magnitudes and/or locations of slip events derived from different types of modeling studies, and also when similar types of models have different discretization mesh.

Slow slip doubtless does vary significantly as a function of location on the plate interface, and GPS displacements are most sensitive to slip occurring nearest the measurement site. The patch model is overdamped and reduces misfit associated with spatially varying slip by locating the slip source at greater distance from the measurements. The greater distance to the source also forces moment release to be larger to approximate the surface displacement magnitudes. Slip vectors on many of the rectangular patch models are tens of cm, and the cumulative slow slip on the interface can far exceed the relative plate motion over a similar time span (a physically unlikely scenario). Because the discretized model constrains slow slip not to exceed the accumulated slip deficit, the discretized

models favor slip nearer the GPS sites that reproduces surface displacement with smaller moment release. We validate this assertion by modifying the discretized slow slip inversion to minimize both model misfit and the resulting estimate of moment release. Results of such a calculation, included in the final column of Table 2, demonstrate that requiring slow slip not to exceed the available slip deficit yields about the same result as a minimum-moment solution.

In the context of this paper, it is very important to recognize that finding substantial differences in the two end-member approaches to modeling slow slip is actually a desired result. If the two end-member models of slow slip produce end-member estimates of slip deficit, then our range of estimates of the seismogenic potential derived from these two models should accurately reflect the range of possible seismic hazard in the Guerrero gap. That said, ideally one would also like to distinguish one or the other model as being a more accurate representation of slow slip behavior. The smaller misfit and reduced damping of the discretized models, coupled with the moment-minimization constraints, would imply that the discretized models more accurately reflect the slip behavior (although estimates of slip and moment release are conservative in the sense that slip is biased toward zero in regions far from GPS constraint).

6.2 Implications for slip processes

The analysis performed here provides some new clues to the processes that drive slow slip. The observation that events in Guerrero are quasi-periodic with annual period is one important hint. Location information provides another clue to the slip process, and timing relations that relate to likely propagation of slip offer a third important puzzle piece.

Rate- and state-dependent frictional modeling (Liu & Rice 2005) suggests that two elements are needed to generate fault behavior similar to slow slip events: (1) small along-strike variations in frictional properties on the fault, and (2) some sort of transient stress process. In Liu & Rice's (2005) simulations, postseismic slip following the previous large megathrust event provided the stress transient, but transient stress might also result from smaller earthquakes on or near the plate boundary. The 1996–97 Bungo Channel event (Hirose et al. 1999) initiated soon after a pair of nearby M_w=6.7 earthquakes, although some models suggest part of the slow slip initiated $\sim$100 km away and propagated toward the earthquakes (Miyazaki et al. 2003). In Guerrero, the 1996 event may have been postseismic slip associated with the 1995 M_w=7.3 Copala earthquake, but timing constraints are poor. The 2002 event was preceded by the M_w 6.0 Coyuca earthquake, an upper plate normal faulting event, and differences in timing of deformation at different sites in Guerrero suggest that slip initiated and propagated outward from somewhere near that earthquake (Kostoglodov et al. 2003). Significantly however,

no M_w>5 earthquake occurred anywhere near the plate bounding thrust in the months preceding the 1998 event, and smaller slip events similarly have no strong correlation with earthquake activity.

The 12.0±0.3 month periodicity of Guerrero events suggests an alternative source of transient stress. Annual periodicity may indicate that slip is also somehow forced or modulated by seasonal variations in mass loading at the Earth's surface. Lowry (2006) examines fault stress changes due to continental hydrologic mass loading and finds peak-to-peak variations of up to 300 Pa in shear stress and even larger in normal stress. While this is only about 5 to 20% of the annual tectonic shear stress accumulation, Lowry (2006) also shows that resonance of fault slip and stress is most robust for frictional conditions near the base of the seismogenic zone, where frictional properties prescribe a resonant frequency of order one year. Most locations where slow slip has been documented exhibit periodic behavior. Cascadia events have a recurrence interval of 13.9±1 months near the northern Puget basin, 10.9±1.2 months in northern California and Oregon (Szeliga et al. 2004), and ∼14 month periodicity in the Explorer plate region that is ∼6 months out of phase with the Puget activity (Malone et al. 2004). Events in the Shikoku region of Japan occur once every six months with alternating directions of propagation (Obara et al. 2004). Resonant periods depend on the a and b frictional parameters on the fault, and as different faults likely have slightly different frictional properties near the base of the seismogenic zone it is not surprising that slow slip elsewhere would be excited by environmental stress at other periods. 13.9 months, for example, is approximately the period of the pole tide (Shen et al. 2005), and loading by the atmosphere, oceans and continental hydrology all contain significant power at periods other than annual.

If we are correct in inferring that slow slip represents a resonance effect arising from fault frictional response, this would also imply that slip must initiate within the velocity weakening (i.e., seismogenic) zone (Perfettini et al. 2001) near the frictional transition where $(b - a)$ becomes vanishingly small (Lowry 2006). Some researchers (e.g., Dragert et al. 2001) have suggested previously that slow slip must occur downdip of the seismogenic zone to prevent slip accelerating to earthquake rupture speeds, but in fact area of slip must exceed a threshold defined by stiffness properties on the fault in order for rupture to initiate. Location of slip is ambiguous in the models presented here, but a substantial fraction of slow slip occurring within the velocity-weakening frictional regime is at least consistent with the GPS observations.

One puzzling aspect of the observations is the question of why slip and moment release of Guerrero events is so variable if slip represents a periodic resonance phenomenon. Modeling presented here suggests a possible answer to that question as well. Large events in Guerrero differ from the smaller events in that they require a significant contribution of moment release from regions downdip of the seismogenic zone, where resonance cannot occur. This modeling result is reinforced by a relative lack

of trenchward displacement at inland sites during smaller events and by the later occurrence of deformation at inland sites than at coastal sites during the larger (1998, 2002 and 2003) events (Table 1). This behavior suggests the possibility that slip is consistent from one year to the next on the shallow resonating patch, but in some years significant slip propagates downdip into the velocity-strengthening zone, while in other years it does not. A potential problem with this interpretation is that simulated slip events (e.g., Liu & Rice 2005) apparently do not propagate below the frictional transition. However, simulated events also do not reproduce periodicity or rapid along-strike propagation observed in the real Earth, so this may simply reflect parameterization of the rate-state frictional models. Slip clearly propagates from velocity-weakening to velocity-strengthening frictional regimes in postseismic signals (e.g., Hutton et al. 2001), so it is not unreasonable to expect similar behavior from slow slip events.

6.3 Upper plate strain partitioning

Modeling for this study assumes negligible permanent deformation of the North American upper plate on the short timescale of measurements. Nevertheless, steady-state velocities can be used to infer partitioning of oblique relative plate motion into upper plate strike-slip faulting. Figure 10 shows the sinistral component of residual GPS site velocity relative North America versus distance from the trench. The three candidate fault zones for partitioning of upper plate strike-slip motion, shown in map view in Figure 1, are superimposed. Most of the scatter in velocity estimates reflects uncertainty in separating slow slip displacement from steady-state velocity at campaign GPS sites. Velocities of the CGPS sites are more tightly clustered, averaging about 8 mm yr^{-1} near the coast (65–95 km from the trench), with scatter that generally reflects the eastward increase in sinistral component of relative plate motion. Sinistral velocities drop to 5.6 mm yr^{-1} at OAXA (200 km from the trench), 1.8 mm yr^{-1} at IGUA (250 km) and 0.2 mm yr^{-1} at YAIG (300 km). POSW appears to have a 1.1 mm yr^{-1} dextral velocity, but this is likely an artefact of Popocatépetl volcanic deformation. The distribution of CGPS sites is not adequate to distinguish deformation on the Atoyac fault from that of the Chapala-Oaxaca fault zone, but we can infer with some certainty that all of the $\sim$8 mm yr^{-1} sinistral motion is accommodated on those two faults. Motions at OAXA and IGUA imply that the COFZ accommodates more strike slip than the Atoyac fault. Márquez-Azúa & DeMets (2003) suggest the Chapala-Tula fault zone may accommodate up to 4 mm yr^{-1}, but we find no evidence to support that in Guerrero network data. Structural and paleomagnetic investigations (Suter et al. 2001; Ruiz-Martínez et al. 2000) indicate only a few tenths of a mm yr^{-1} displacements across the Chapala-Tula faults, consistent with our results.

Darby & Beavan (2001) observe that accumulation of upper plate shear strain is largest over the transition from locked to slipping on the subduction interface at oblique subduction boundaries. Consequently, above the slip transition is a natural location for strike-slip fault structures (such as the Wellington fault in their study) to develop. In southern Mexico, there are two slip transitions at two different timescales. One transition separates constant free slip from nearly complete coupling during the time interval between large slow slip events. That transition approximately corresponds to the location of the Chapala-Oaxaca fault zone. A second transition separates the seismogenic zone, which remains partially coupled between large-magnitude megathrust earthquakes, from the region of intermittent slow slip. The latter transition is located nearer the Atoyac fault.

6.4 Seismic potential of the Guerrero Gap

Based largely on the observation that coastal CGPS sites such as CAYA and ACAP accumulate little net deformation, some studies suggest that Guerrero slow slip events release nearly all of the interseismic strain accumulation (e.g., DeMets et al. 2004). The implications of this hypothesis are societally important: If Guerrero is a seismic gap because shallow slip occurs aseismically, the seismogenic potential of the Guerrero segment may be much smaller than the M_w 8.1–8.4 event inferred prior to the recognition of slow slip (e.g., Suárez et al. 1990). Our models suggest that slow slip may indeed occur within the seismogenic zone, and/or that parts of the shallow Guerrero thrust slip aseismically in steady-state (Figures 7–8). However, the important question from a seismic hazard perspective is not whether aseismic slip occurs, but rather, "How much strain energy remains available for earthquake release at the end of the seismic cycle?"

We examine this quantitatively by integrating the slip deficit predicted by the modeling. Slip deficit at a given location on the plate boundary is defined as $(2005.00 - 1992.25)\vec{\Phi}\vec{V}_{\mathrm{rpm}} - \sum_{j=1}^{8} \vec{S}_{0j}$ (i.e., total backslip during the 1992.25 to 2005.00 interval of GPS measurement, less slip in each of the eight slow slip events). We integrate the slip deficit within the seismogenic portion of the Guerrero gap, delimited by Acapulco on the east and the village of Papanoa on the west (i.e., the unruptured NW Guerrero segment shown inset of Figure 1). The integral of slip deficit is converted to strain moment using the same shear rigidity $\mu = 2 \times 10^{10}$ assumed in deformation modeling, and then scaled by a factor of 7.4 (implicitly assuming that slip during the period 1992.25 to 2005.0 is representative of slip during the period 1911 to 2005). The resulting estimate of seismogenic potential has magnitude equivalent M_w=8.01 in the case of the discretized model, and M_w=7.91 in the case of the rectangular patch model.

For this application, extreme differences between the two end-member models of transient slip are actually desirable because they afford a means of approximating upper- and lower-bound estimates

of the final slip deficit. The two estimates of seismogenic potential differ by less than 30%, even though the discretized model locates most slow slip within the seismogenic zone and the rectangular patch model locates virtually all of the slip further downdip. Interestingly, the rectangular patch model produces a smaller seismogenic potential despite predicting negligible seismogenic zone slow slip. This is because the patch model requires more aseismic slip in the seismogenic zone between slow slip events to balance the total deformation observed at the GPS sites (compare Figures 8a and 8b). Hence, if slip behavior during the GPS measurement period is representative of the interseismic period, the M_w=7.9–8.0 seismogenic potential of the Guerrero gap can be considered a robust estimate.

The model estimates of potential moment release presented here are consistent with moment release during the 1911 (M_S=7.8) earthquake but smaller than hazard estimates based on extrapolation of earthquake behavior elsewhere on the Cocos-North America plate boundary. The discrepancy suggests that the Guerrero gap is a gap in part because an unusually large fraction of the shallow fault on this segment has velocity strengthening frictional conditions, and/or resonant slip in the velocity-weakening zone is a significant fraction of total moment release. Although projected moment release is smaller than previously estimated, the prospect of a M_w=7.9–8.0 earthquake still poses a significant threat of property damage and loss of life to the $\sim$20 million inhabitants of Mexico City, Acapulco and other large cities in Guerrero state.

7 CONCLUSIONS

Previous studies of GPS deformation in Guerrero have examined slow slip events that produced large surface displacements in 1996, 1998 and 2002. In this study we find evidence for additional smaller events in 1999, 2000, 2001, 2003 and 2004. The approximately annual (12.0$\pm$0.3 months) recurrence of these events is similar to that observed for slow slip in Cascadia and Japan. Displacements during the smaller events have large SNR, and directions are similar to the larger events. The directions and time-dependence are consistent with expectations for slow slip and inconsistent with surface mass loading deformation or other annual signals. Surface displacements vary by nearly an order of magnitude from the largest to smallest events, indicating that they do not simply repeat but rather that each event results from differing amounts and locations of slip on the plate boundary.

We invert for plate boundary slip using two different types of models: (1) uniform slip within a rectangular patch, and (2) variable slip on a discretized surface. The discretized thrust model is regularized by requiring slow slip to be less than or equal to the slip deficit accumulated in inter-event times, resulting in a parameterization that approximately minimizes the total moment release. The discretized model yields a better fit to GPS time series than the patch model and confirms that slip deficit accumulated during inter-event times is sufficient to drive slow slip.

Estimates of the location of slip and total moment release are very different for these two types of models because regularization of the discretized model forces slip to be small and near the GPS sites, whereas the single patch favors models in which slip is larger and more distant. Because slip likely does vary, we expect that the discretized model more accurately reflects the true behavior. However moment release reported for discretized models in Table 2 should be considered a lower bound, because slip may be inadequately sampled outside the Guerrero GPS network.

Slow slip in Guerrero concentrates near the downdip portion of the seismogenic zone. Additional, later-occurring slip further inland (downdip) is required to explain larger events such as in 2002. These observations suggest that (1) slow slip initiates in velocity-weakening frictional conditions (as predicted by resonance theory in rate and state dependent friction models), and (2) slip sometimes (but not always) propagates downdip into the velocity-weakening regime where moment release can be larger. Slip on the plate boundary during inter-event periods is near zero to significant depths (about 45 km) and distances (about 200 km from the trench).

The trench-parallel component of steady-state velocity in Guerrero indicates that, if partitioning of oblique Cocos-North America motion does occur, most of the $\sim$8 mm yr^{-1} of sinistral motion is resolved on the Atoyac and Chapala-Oaxaca fault zones. Strike-slip motion across the Chapala-Tula fault zone is negligible to within uncertainties of a few tenths of a mm.

Integration of the slip deficit on the Guerrero seismogenic zone during the GPS measurement period indicates that, if slip behavior since 1992 is representative of the interseismic period, the Guerrero segment currently has the potential to generate a M_w=7.9 to 8.0 earthquake. This estimate represents a range derived from two very distinct, end-member approaches to modeling slip and so is a robust estimate of the seismic hazard on the Guerrero segment.

8 ACKNOWLEDGMENTS

Early GPS surveys from 1992–2000 were supported by CONACYT grants 1089-T9201, G25842-T and NSF grant EAR-9725712. Funding for sites COYU, CPDP, and DOAR was provided by NSF grant EAR-0125618 with UNAVCO technical support. Jose Antonio Santiago installed, maintained and acquired data from most Guerrero CGPS sites with the financial support of IN102697 (PAPIIT), 4960-T and G25842-T (CONACYT). V.K. and Roger Bilham installed CAYA with NSF major equipment funding. Yehuda Bock provided a receiver for use at YAIG. NASA, Tim Dixon, and Enrique Cabral supported the installation of POSW. The GPS campaign and NSF-funded (CAYA, COYU, CPDP, and DOAR) CGPS data are archived at UNAVCO Inc (http://www.unavco.org). NSF grants EAR-0125618 and EAR-0207820 supported CU investigators. We thank the Servicio Seismológico Nacional and particularly Casiano Jiménez Cruz, Javier Pacheco and Shri Krishna Singh for collect-

ing and processing most of the seismic data used in this research. Precise orbits from the International GPS Service and the Jet Propulsion Laboratory are gratefully acknowledged. We also thank John Wahr for discussions and software used in the load deformation modeling. Some of the figures were generated using the Generic Mapping Tools package (Wessel & Smith 1998).

REFERENCES

Altamimi, Z., Sillard, P., & Boucher, C., 2002, ITRF2000: A new release of the International Terrestrial Reference Frame for Earth science applications, *J. Geophys. Res.*, **107**(B10), doi:10.1029/2001JB000561.

Bassin, C., Laske, G., & Masters, G., 2000, The current limits of resolution for surface wave tomography in North America, *Eos Trans. AGU*, **81**, F897.

Bawden, G. W., Thatcher, W., Stein, R. S., Hudnut, K. W., & Pletzer, G., 2001, Tectonic contraction across Los Angeles after removal of groundwater pumping effects, *Nature*, **412**, 812–815.

Beck, J. V. & Arnold, K. J., 1977, *Parameter Estimation in Engineering and Science*, Wiley, New York.

Blewitt, G., 1989, Carrier phase ambiguity resolution for the Global Positioning System applied to geodetic baselines up to 2000 km, *J. Geophys. Res.*, **94**, 10,187–10,203.

Blewitt, G. & Lavallée, D., 2002, Effects of annual signals on geodetic velocity, *J. Geophys. Res.*, **107**(B7), 2145, doi:10.1029/2003JD004345.

Bürgmann, R., Kogan, M. G., Levin, V. E., Scholz, C. H., King, R. W., & Steblov, G. M., 2001, Rapid aseismic moment release following the 5 December, 1997 Kronotsky, Kamchatka, earthquake, *Geophys. Res. Lett.*, **28**, 1331–1334.

Darby, D. & Beavan, J., 2001, Evidence from GPS measurements for contemporary interplate coupling on the southern Hikurangi subduction thrust and for partitioning of strain in the upper plate, *J. Geophys. Res.*, **106**, 30,881–30,891.

DeMets, C., Gordon, R. G., Argus, D. F., & Stein, S., 1994, Effect of recent revisions to the geomagnetic reversal time scale on estimates of current plate motions, *Geophys. Res. Lett.*, **21**, 2191–2194.

DeMets, C., Brudzinski, M. R., Cabral-Cano, E., Márquez-Azúa, B., & Correa-Mora, F., 2004, Large-scale seismic and aseismic deformation patterns associated with subduction: Constraints from continuous GPS measurements in Mexico, *Eos Trans. AGU*, **85**(47), Abstr. S43D–07.

Douglas, A., Beavan, J., Wallace, L., & Townend, J., 2005, Slow slip on the northern Hikurangi subduction interface, New Zealand, *Geophys. Res. Lett.*, **32**, L16305.

Dragert, H., Wang, K., & James, T. S., 2001, A silent slip event on the deeper Cascadia subduction interface, *Science*, **292**, 1525–1528.

Dziewonski, A. M. & Anderson, D. L., 1981, Preliminary reference Earth model, *Phys. Earth Planet. Inter.*, **25**(4), 297–356.

Fan, Y. & van den Dool, H., 2004, Climate Prediction Center global monthly soil moisture data set at 0.5° resolution for 1948 to present, *J. Geophys. Res.*, **109**(D10102), doi:10.1029/2003JD004345.

Freymueller, J. T., Cohen, S. C., Hreinsdóttir, S., & Suito, H., 2003, Long-term postseismic deformation following the 1964 Alaska earthquake, *Eos Trans. AGU*, **84**(46), Abstr#G22E–03.

Gordeev, E. I., Gusev, A. A., Levin, V. E., Bakhtiarov, V. F., Pavlov, V. M., Chebrov, V. N., & Kasahara, M., 2001, Preliminary analysis of deformation at the Eurasia-Pacific-North America plate junction from GPS data, *Geophys. J. Int.*, **147**(1), 189–198.

Heki, K., Miyazaki, S., & Tsuji, H., 1997, Silent fault slip following an interplate thrust earthquake at the Japan trench, *Nature*, **386**(6625), 595–598.

Hirose, H. & Obara, K., 2005, Repeating short- and long-term slow slip events with deep tremor activity around Bungo channel region, southwest Japan, *Earth Planets Space*, **57**, in press.

Hirose, H., Hirahara, K., Kimata, F., Fujii, N., & Miyazaki, S., 1999, A slow thrust slip event following the two 1996 Hyuganada earthquakes beneath the Bungo Channel, southwest Japan, *Geophys. Res. Lett.*, **26**, 3237–3240.

Hutton, W., DeMets, C., Sánchez, O., Suárez, G., & Stock, J., 2001, Slip dynamics during and after the 9 October 1995 M_w=8.0 Colima-Jalisco earthquake, Mexico, *Geophys. J. Int.*, **146**, 637–658.

Iglesias, A., Singh, S. K., Lowry, A. R., Kostoglodov, V., Larson, K. M., Franco-Sanchez, S. I., & Mikumo, T., 2004, The silent earthquake of 2002 in the Guerrero seismic gap, Mexico (M_w=7.4): inversion of slip on the plate interface and some implications, *Geofisica Int.*, **43**(3), 309–317.

Johnson, C. A. & Harrison, C. G. A., 1990, Neotectonics in central Mexico, *Phys. Earth Planet. Inter.*, **64**, 187–210.

Julian, B., 2002, Seismological detection of slab metamorphism, *Science*, **296**, 1625–1626.

Kawasaki, I., Asai, Y., Tamura, Y., Sagiya, T., Mikami, N., Okada, Y., Sakata, M., & Kasahara, M., 1995, The 1992 Sanriku-Oki, Japan, ultra-slow earthquake, *J. Phys. Earth*, **43**(2), 105–116.

Kostoglodov, V. & Ponce, L., 1994, Relationship between subduction and seismicity in the Mexican part of the Middle America Trench, *J. Geophys. Res.*, **99**(B1), 729–742.

Kostoglodov, V., Bandy, W., Domínguez, J., & Mena, M., 1996, Gravity and seismicity over the Guerrero seismic gap, Mexico, *Geophys. Res. Lett.*, **23**, 3385–3388.

Kostoglodov, V., Singh, S. K., Santiago, J. A., Franco, S. I., Larson, K. M., Lowry, A. R., & Bilham, R., 2003, A large silent earthquake in the Guerrero seismic gap, Mexico, *Geophys. Res. Lett.*, **30**(15), doi:10.1029/2003GL017219.

Larson, K. M., Lowry, A. R., Kostoglodov, V., Hutton, W., Sánchez, O., Hudnut, K., & Suárez, G., 2004, Crustal deformation measurements in Guerrero, México, *J. Geophys. Res.*, **109**(B4), B04409.

Lichten, S. & Border, J., 1987, Strategies for high precision GPS orbit determination, *J. Geophys. Res.*, **92**, 12,751–12,762.

Linde, A. T. & Silver, P. G., 1989, Elevation changes and the great 1960 Chilean earthquake: Support for aseismic slip, *Geophys. Res. Lett.*, **16**(11), 1305–1308.

Liu, Y. & Rice, J. R., 2005, Aseismic slip transients emerge spontaneously in three-dimensional rate and state modeling of subduction earthquake sequences, *J. Geophys. Res.*, **110**(B8), B08307.

Lowry, A. R., 2006, Resonant slow fault slip in response to climatic load stress, *Nature*, **in press**.

Lowry, A. R., Larson, K. M., Kostoglodov, V., & Bilham, R. G., 2001, Transient slip on the subduction interface in Guerrero, southern Mexico, *Geophys. Res. Lett.*, **28**, 7909–7922.

Lowry, A. R., Tamisiea, M. E., & Latychev, K., 2006, Variability of Earth's elastic response to mass loading, *Geophys. Res. Lett.*, **in prep**.

Malone, S., Rogers, G., Dragert, H., McCausland, W., & Johnson, D., 2004, Review of Episodic Tremor and Slip in Cascadia, *Eos Trans. AGU*, **85**(47), Abstr#S53A–0188.

Márquez-Azúa, B. & DeMets, C., 2003, Crustal velocity field of Mexico from continuous GPS measurements, 1993 to June 2001: Implications for the neotectonics of Mexico, *J. Geophys. Res.*, **108**(B9), doi:10.1029/2002JB002241.

Melbourne, T. I. & Webb, F. H., 2003, Slow but not quite silent, *Science*, **300**, 1886–1887.

Melbourne, T. I., Szeliga, W. M., Miller, M. M., & Santillan, V. M., 2005, Extent and duration of the 2003 Cascadia slow earthquake, *Geophys. Res. Lett.*, **32**(L04301), doi:10.1029/2004GL021790.

Miller, M. M., Melbourne, T., Johnson, D. J., & Sumner, W. Q., 2002, Periodic slow earthquakes from the Cascadia subduction zone, *Science*, **295**, 2423.

Miyazaki, S., McGuire, J. J., & Segall, P., 2003, A transient subduction zone slip episode in southwest Japan observed by the nationwide array, *J. Geophys. Res.*, **108**(B2), Art#2087.

Nikolaidis, R. M., 2002, *Observation of geodetic and seismic deformation with the Global Positioning System*, Ph.D. thesis, Univ. of Calif., San Diego.

Obara, K., Hirose, H., Yamamizu, F., & Kasahara, K., 2004, Episodic slow slip events accompanied by non-volcanic tremors in southwest Japan subduction zone, *Geophys. Res. Lett.*, **31**(23), Art#L23602.

Okada, Y., 1985, Surface deformation due to shear and tensile faults in a half-space, *Bull. Seismol. Soc. Am.*, **75**, 1135–1154.

Ozawa, S., Murakami, M., & Tada, T., 2001, Time-dependent inversion study of the slow thrust event in the Nankai trough subduction zone, *J. Geophys. Res.*, **106**(B1), 787–802.

Ozawa, S., Hatanaka, Y., Kaidzu, M., Murakami, M., Imakiire, T., & Ishagaki, Y., 2004, Aseismic slip and low-frequency earthquakes in the Bungo channel, southwestern Japan, *Geophys. Res. Lett.*, **31**(7), Art#L07609.

Pardo, M. & Suárez, G., 1995, Shape of the subducted Rivera and Cocos plates in southern Mexico: Seismic and tectonic implications, *J. Geophys. Res.*, **100**, 12,357–12,373.

Perfettini, H., Schmittbuhl, J., Rice, J. R., & Cocco, M., 2001, Frictional response induced by time-dependent fluctuations of the normal loading, *J. Geophys. Res.*, **106**(B7), 13,455–13,472.

Protti, M., Gonzalez, V., LaFemina, P., Dixon, T., Kato, T., Iinuma, T., Miyazaki, S., Obana, K., Kaneda, Y., & Schwarz, S., 2005, Possible Slow Slip Event within the Seismogenic Zone, Nicoya Peninsula, Costa Rica, *Geophys. Res. Lett.*, **in press**, 14,133–14,159.

Rogers, G. & Dragert, H., 2003, Episodic tremor and slip on the Cascadia subduction zone: The chatter of silent slip, *Science*, **300**, 1942–1943.

Ruiz-Martínez, V. C., Osete, M. L., Vegas, R., nez Aguilar, J. I. N., Urrutia-Fucugauchi, J., & Tarling, D. H.,

2000, Palaeomagnetism of Late Miocene to Quaternary volcanics from the eastern segment of the Trans-Mexican Volcanic Belt, *Tectonophysics*, **318**(1–4), 217–233.

Savage, J. C., 1983, A dislocation model of strain accumulation and release at a subduction zone, *J. Geophys. Res.*, **88**, 4984–4996.

Shen, Z. K., Wang, Q. L., Bürgmann, R., Yongge, W., & Ning, J., 2005, Pole-tide modulation of slow slip events at circum-Pacific subduction zones, *Bull. Seismol. Soc. Am.*, **95**(5), 2009–2015.

Suárez, G., Monfret, T., Wittlinger, G., & David, C., 1990, Geometry of subduction and depth of the seismogenic zone in the Guerrero gap, Mexico, *Nature*, **345**, 336–338.

Suter, M., Martinez, M. L., Legorreta, O. Q., & Martinez, M. C., 2001, Quaternary intra-arc extension in the central Trans-Mexican volcanic belt, *Geol. Soc. Am. Bull.*, **113**(6), 693–703.

Szeliga, W., Melbourne, T. I., Miller, M. M., & Santillan, V. M., 2004, Southern Cascadia episodic slow earthquakes, *Geophys. Res. Lett.*, **31**(16), L16602.

Thatcher, W., 2001, Silent slip on the Cascadia subduction interface, *Science*, **292**, 1495–1496.

Wahr, J. M., Molenaar, M., & Bryan, F., 1998, Time variability of the Earth's gravity field: Hydrological and oceanic effects and their possible detection using GRACE, *J. Geophys. Res.*, **103**(B12), 30205–30230.

Wessel, P. & Smith, W. H. F., 1998, New, improved version of Generic Mapping Tools released, *Eos Trans. AGU*, **79**(47), 579.

Yoshioka, S., Mikumo, T., Kostoglodov, V., Larson, K. M., Lowry, A. R., & Singh, S. K., 2004, Interplate coupling and a recent aseismic slow slip event in the Guerrero seismic gap of the Mexican subduction zone, as deduced from GPS data inversion using a Bayesian information criterion, *Phys. Earth Planet. Inter.*, **146**, 513–530.

Zumberge, J., Heflin, M., Jefferson, D., Watkins, M., & Webb, F., 1997, Precise point positioning for the efficient and robust analysis of GPS data from large networks, *J. Geophys. Res.*, **102**, 5005–5018.

This paper has been produced using the Blackwell Scientific Publications GJI LaTeX2e class file.

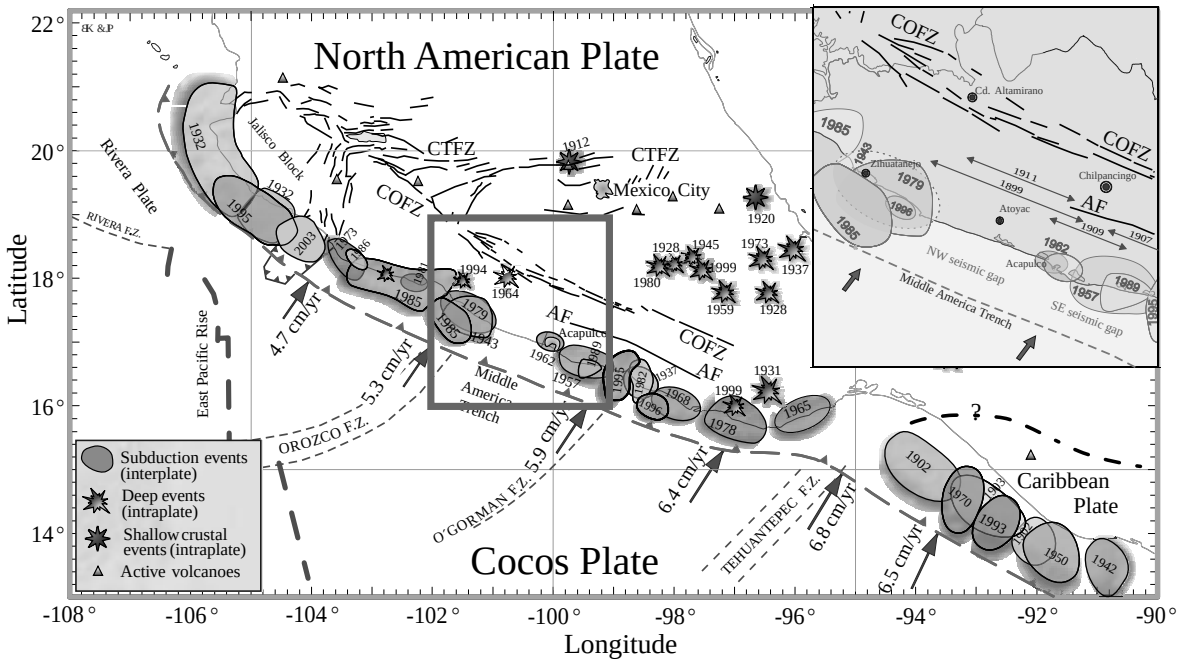

Figure 1. Seismotectonics of southern Mexico. Arrows indicate direction and magnitude of NUVEL1-A relative plate motion (DeMets et al. 1994). Major earthquake slip zones are shown with year of the event. Dark gray box shows location of inset map, which enlarges the setting of the Guerrero seismic gap. Inferred extent of rupture for earthquakes that predate seismic instrumentation are indicated by double-arrowed lines. AF denotes Atoyac fault; COFZ: Chapala-Oaxaca fault zone; CTFZ: Chapala-Tula fault zone after Johnson & Harrison (1990).

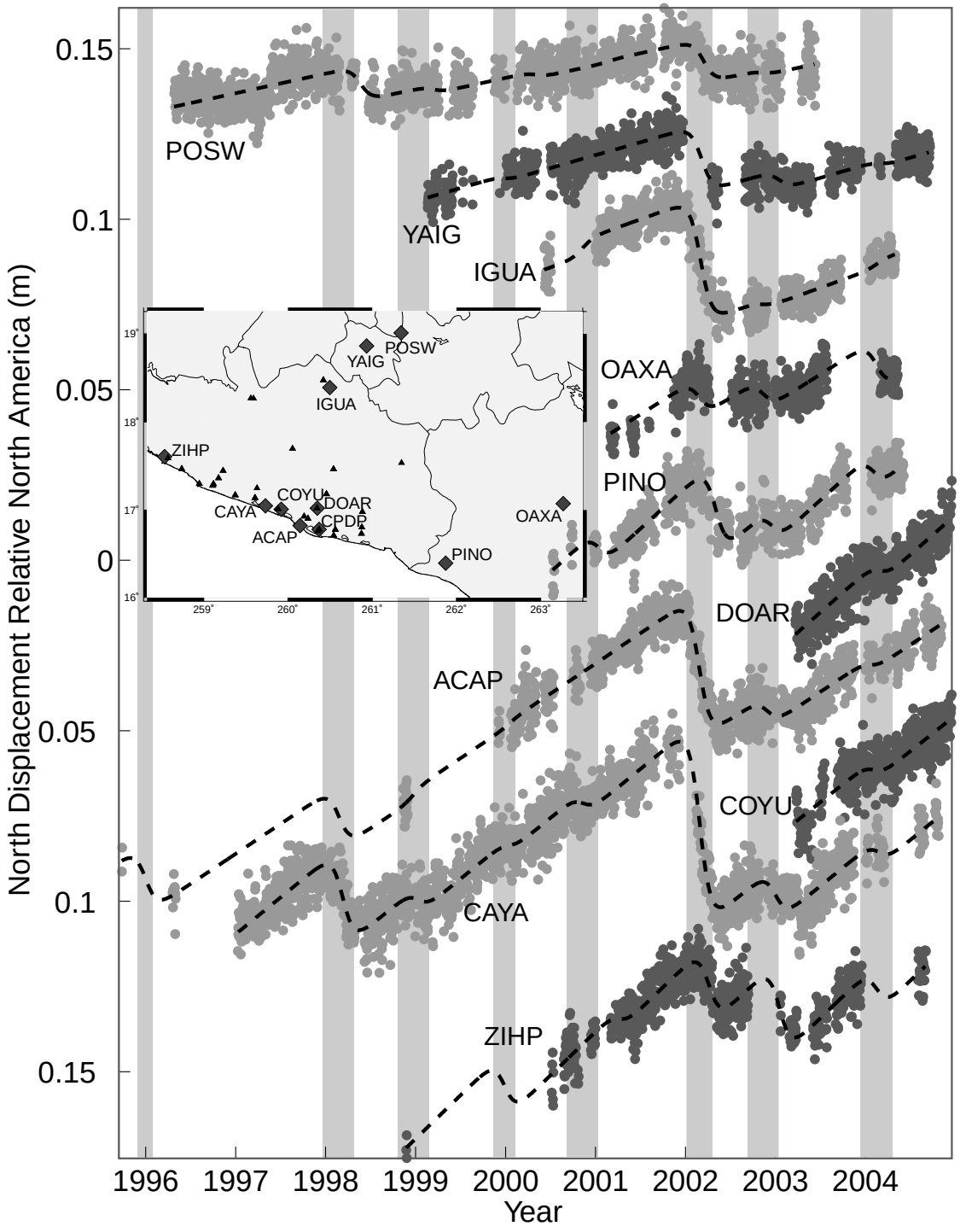

Figure 2. Example time series of GPS north coordinates (North America fixed). Filled circles are measured daily coordinates and dashed lines are best-fit functions of the form given by equation (1). Inset shows map locations of the continuous (diamond) and campaign (triangle) GPS sites in the Guerrero network. Light gray stripes indicate timing of anomalous transient motions visible in the GPS time series.

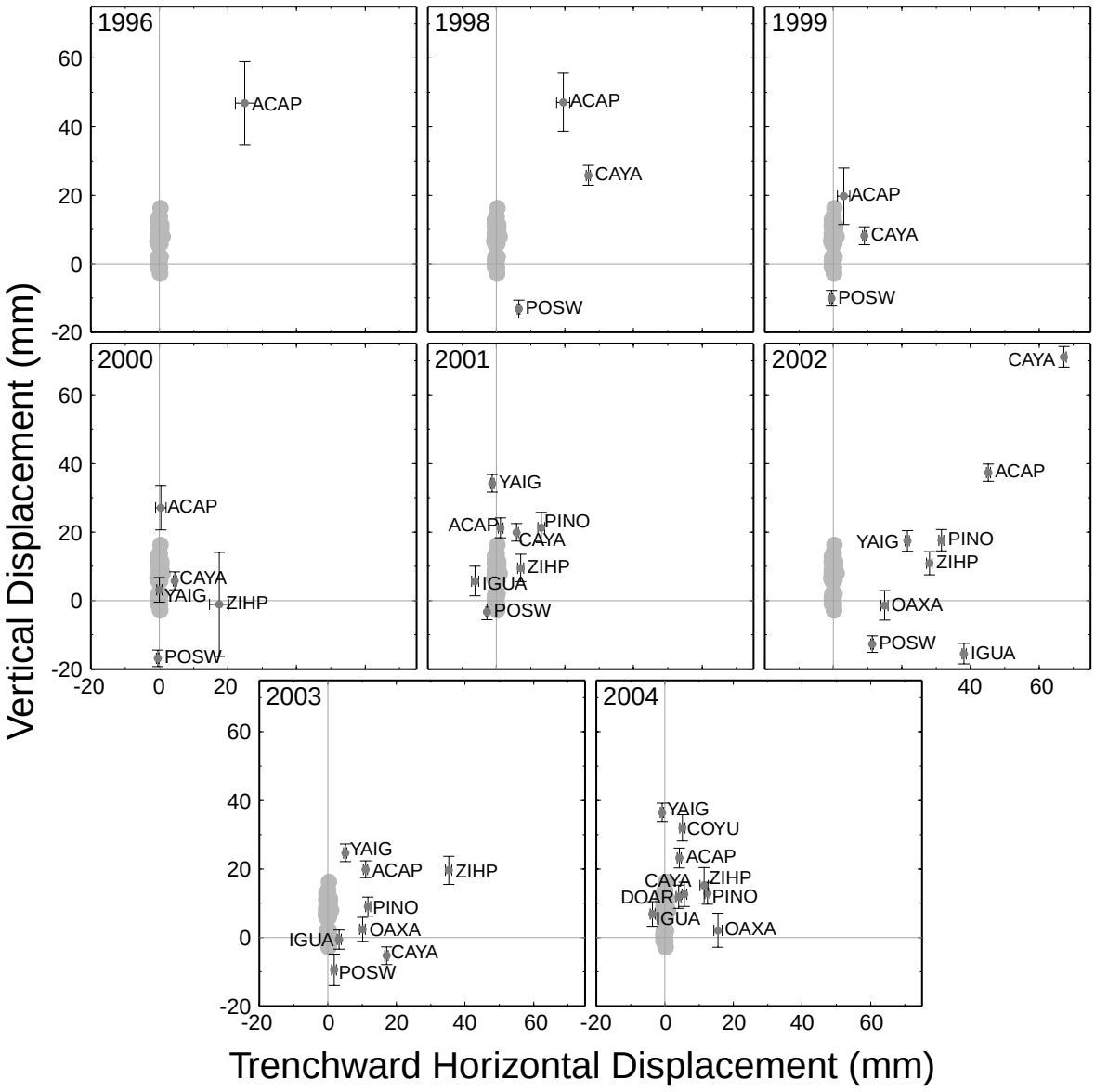

Figure 3. Vertical versus trenchward components of displacement during events identified from HTF offset analysis. Dark grey circles denote best-fit event displacement with one-sigma error bars. “Cloud” of light grey circles indicates displacements derived from similar analysis of a model of deformation response to continental hydrology. Approximate event timing is denoted in the upper left-hand corner of each subplot.

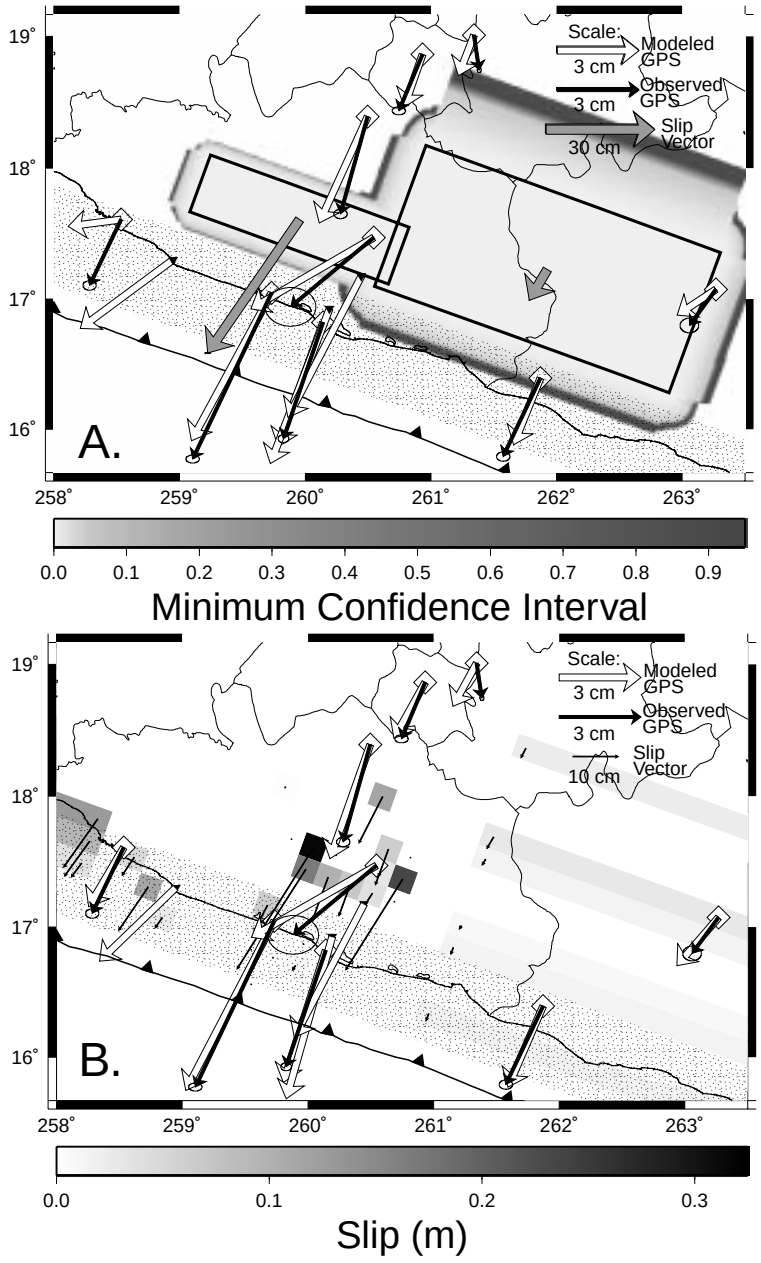

Figure 4. Measured and modeled anomalous displacement during the 2002 slow slip event. Thick black vectors, with 95% confidence ellipse, represent transient displacement from fitting equation (1) to the observed time series. White vectors are from the best-fit model of slow slip. Stippled area approximates the seismogenic zone that produced past great earthquakes. (a) Model using two rectangular patches. Grayscale contours indicate minimum confidence interval of all grid-searched slip models that activated a particular location on the plate boundary; rectangles are surface-projected best-fit slip model. Large gray vector denotes best-fit slip direction. (b) Discretized model of variable slip. Thin black vectors indicate best-fit slip on the gridded megathrust.

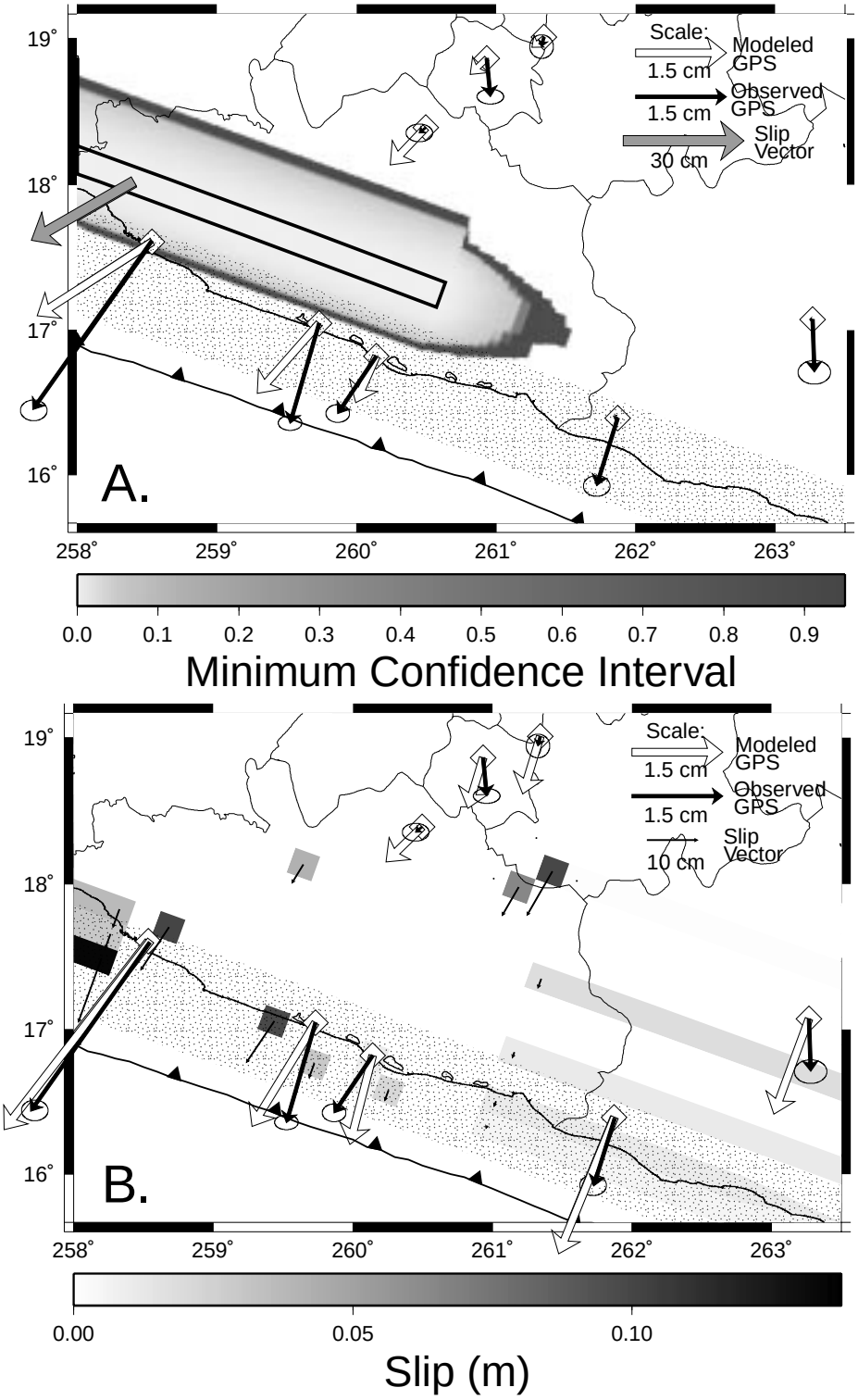

Figure 5. Measured and modeled anomalous displacement during the 2003 slow slip event. See Figure 4 caption for further description.

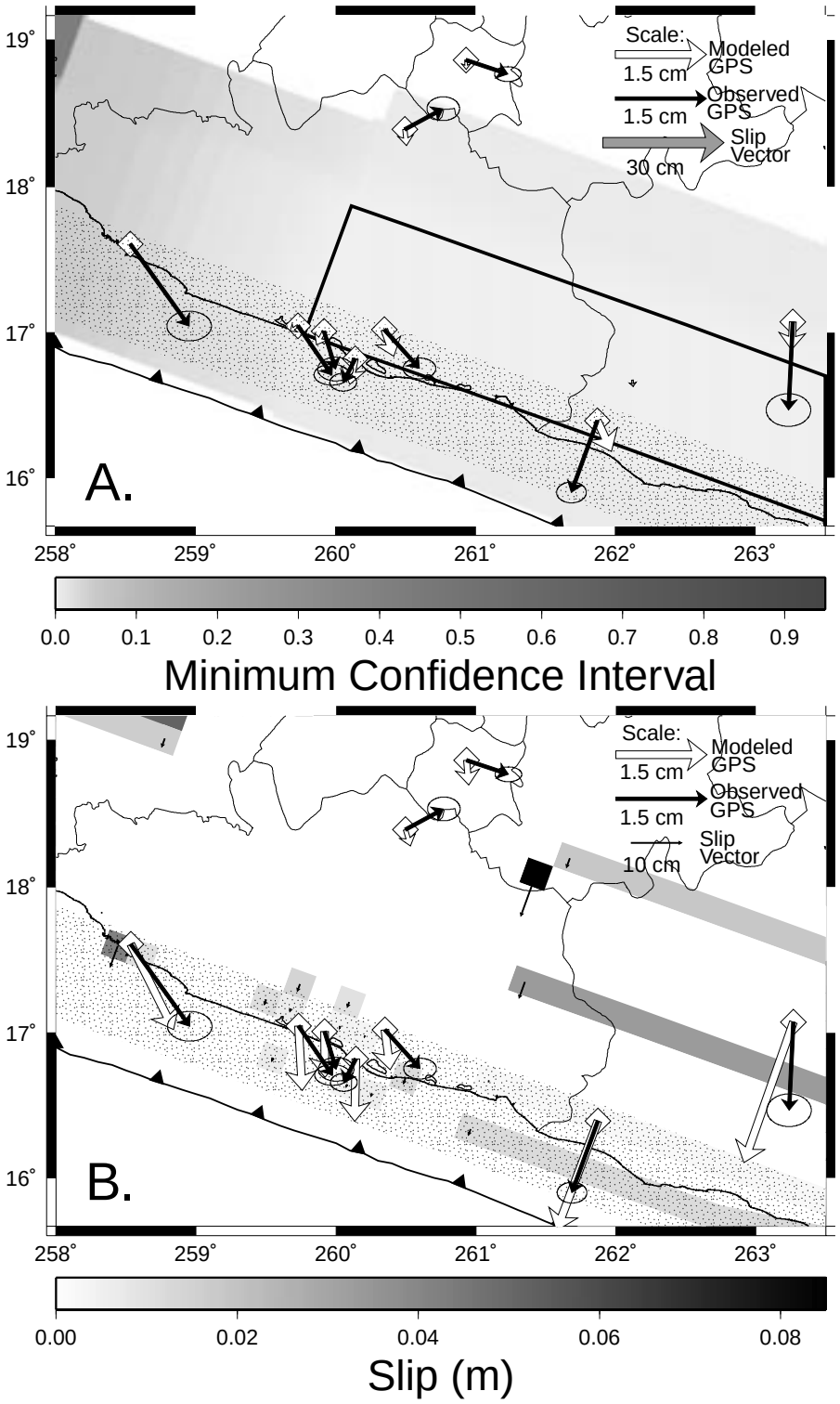

Figure 6. Measured and modeled anomalous displacement during the 2004 slow slip event. See Figure 4 caption for further description.

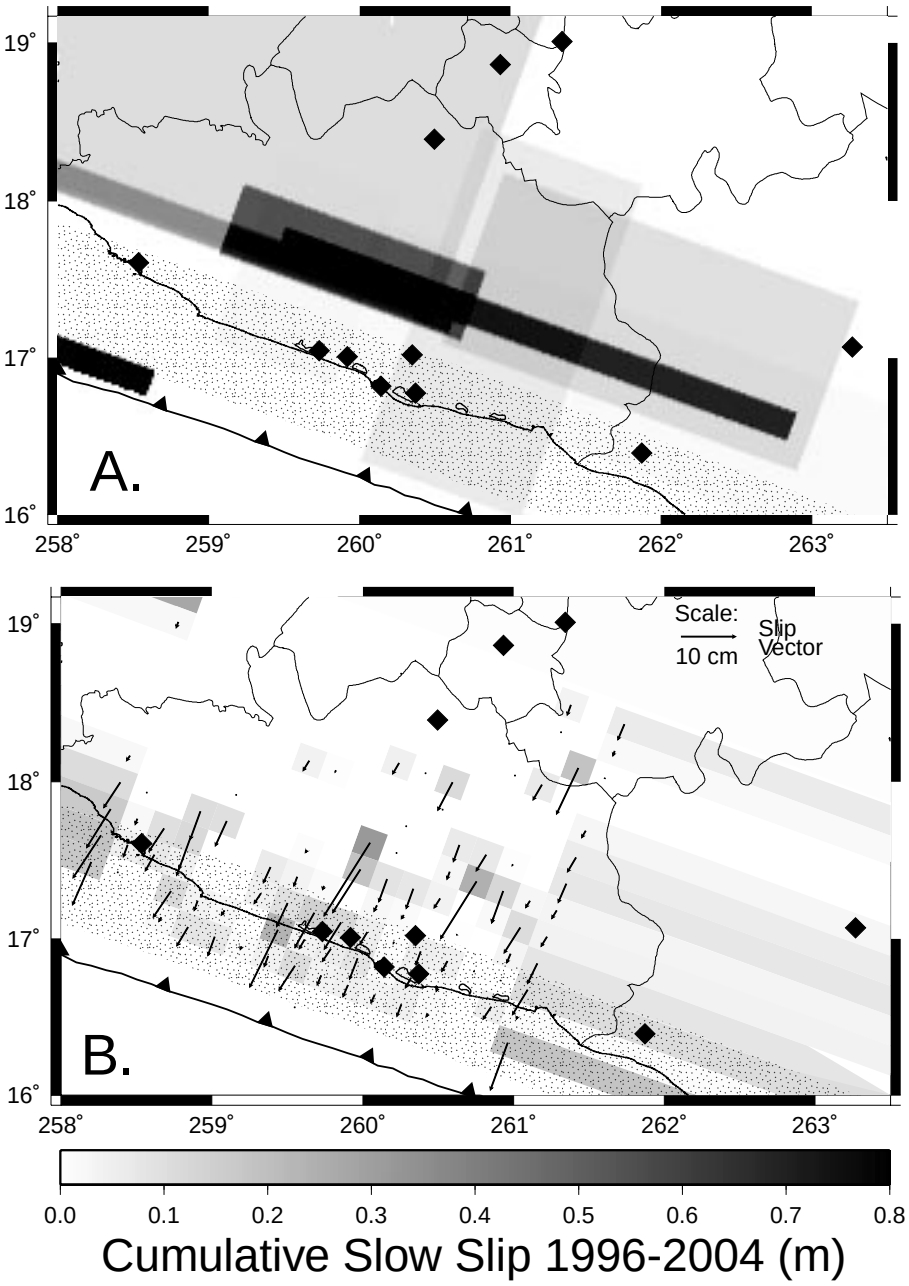

Figure 7. Cumulative slip during slow events, modeled using (a) rectangular patches and (b) a discretized fault surface. Black diamonds show locations of continuous GPS sites.

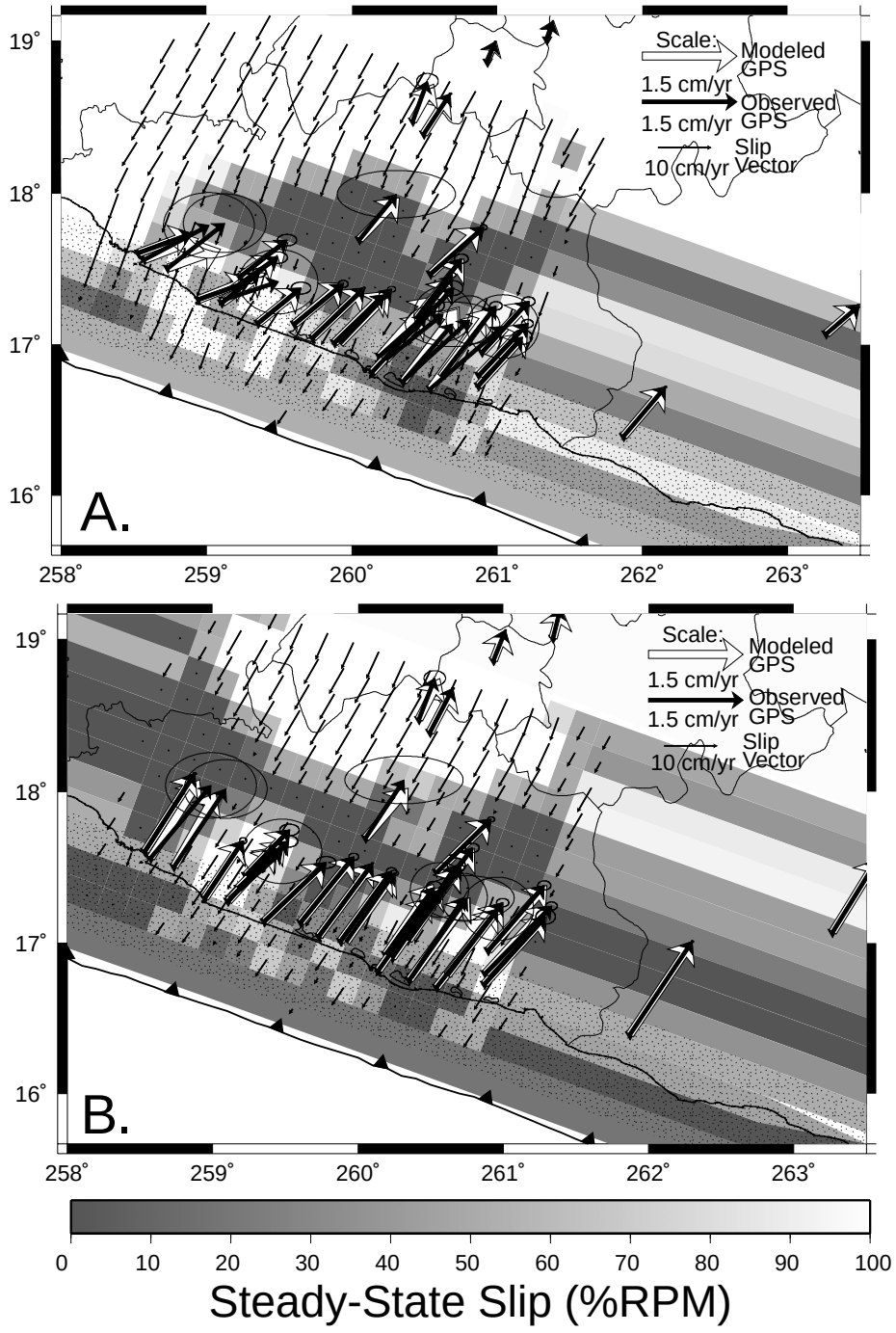

Figure 8. Steady-state slip models. White vectors represent best-fit velocity model; black vectors (with 95% error ellipses) are residual velocity after subtracting the slow slip models. Thin black vectors indicate best-fit steady-state slip projected from the gridded plate boundary to the surface. Grayscale shading represents slip as a fraction of NUVEL-1A relative plate motion. (a) Steady-state slip from residuals of the rectangular patch model of slow slip. (b) Slip from residuals of the discretized slow slip model.

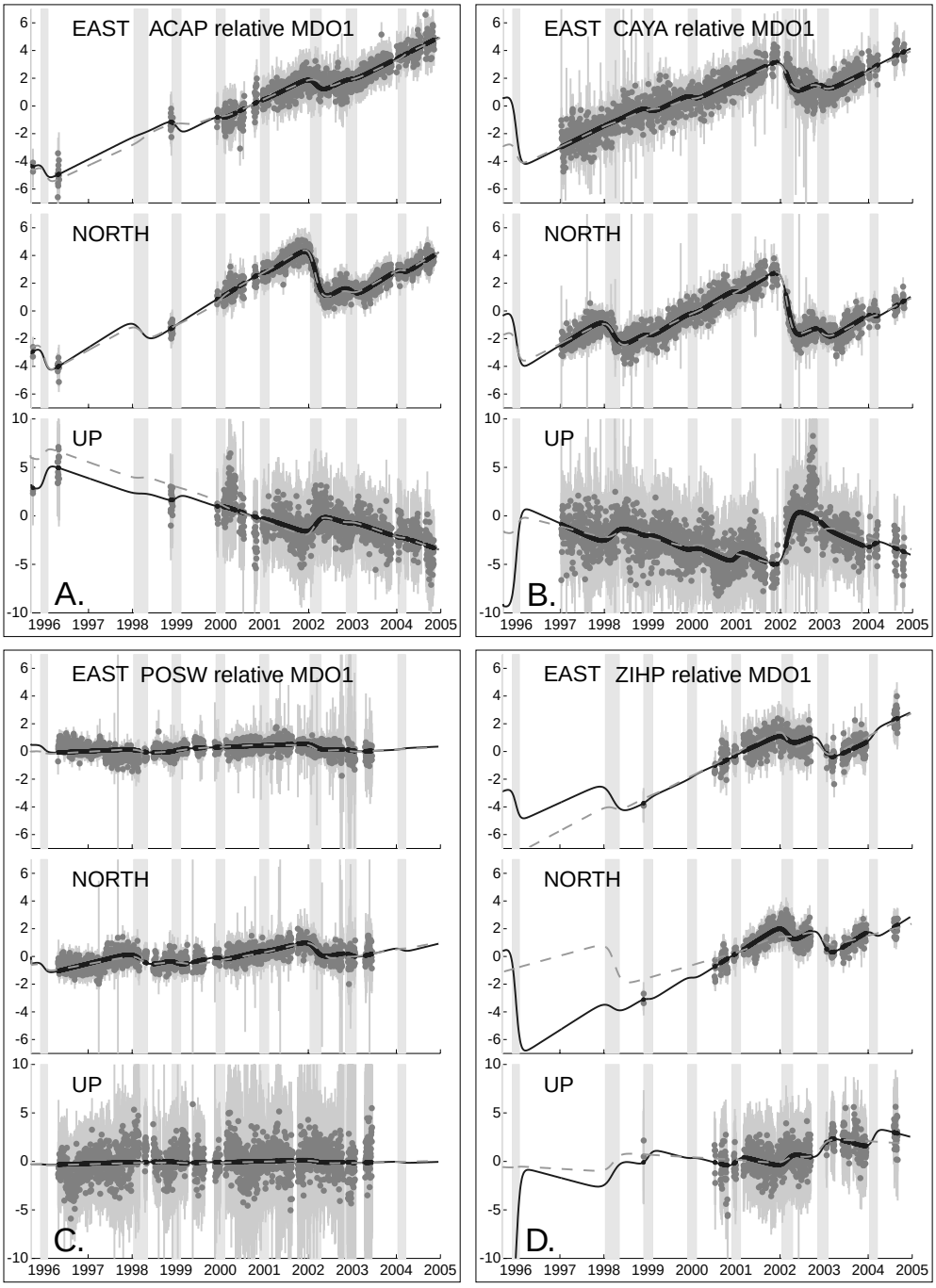

Figure 9. Example best-fit model time series of baseline coordinates relative MDO1 for (a) ACAP, (b) CAYA, (c) POSW, and (d) ZIHP. Gray circles are GPS coordinates, shown with scaled 95% uncertainties (thin light gray bars). Black line is the best-fit discretized model time series for displacement at each site; the dashed gray line superimposed is the corresponding best-fit model of rectangular patches. Very light gray bands denote periods of transient displacement.

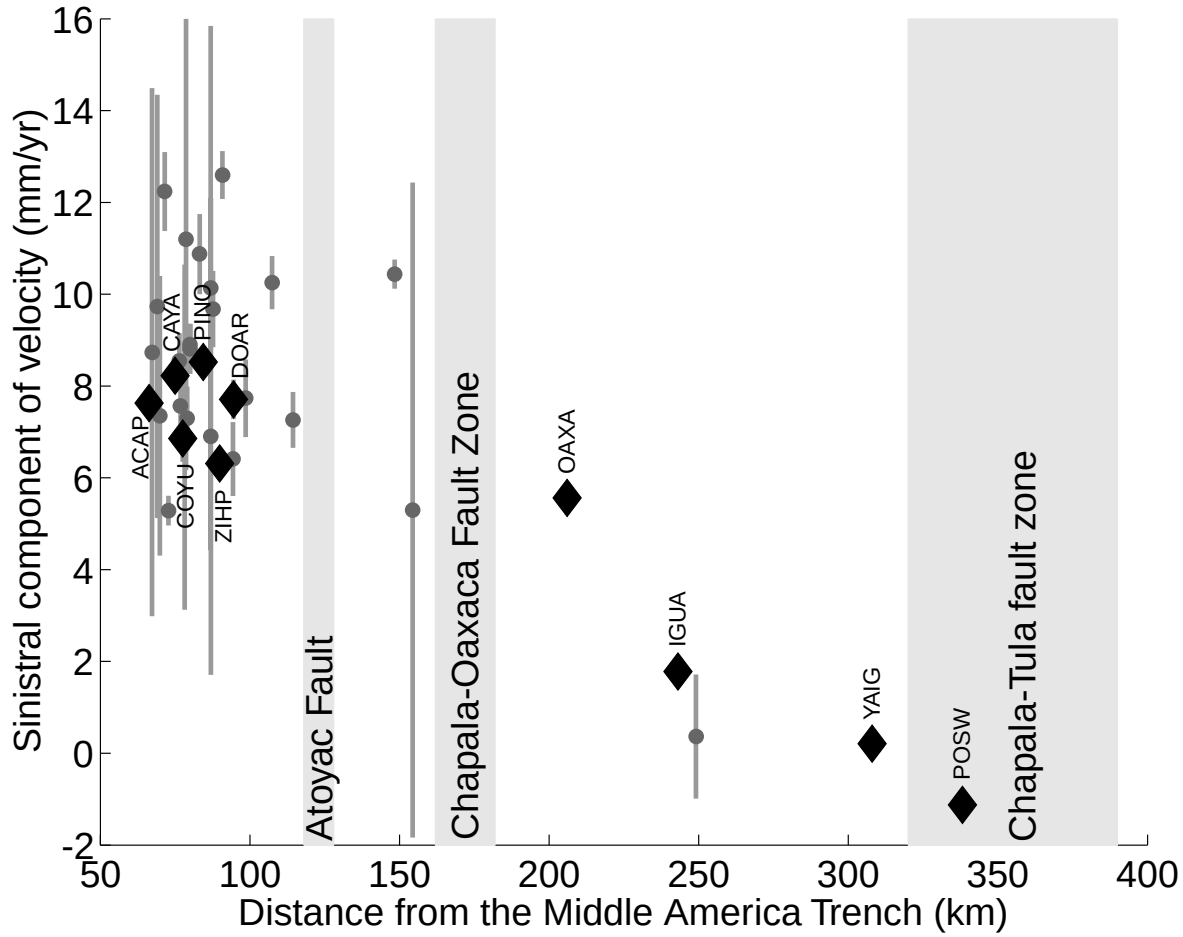

Figure 10. Trench-parallel component of steady-state velocity relative stable North America, with standard error bars. Gray circles denote campaign sites; CGPS sites (larger black diamonds) are labeled. Sinistral motion is positive. Gray bands denote approximate locations of fault zones discussed in the text. Transient displacements from the discretized model are subtracted from the GPS time series prior to estimating velocity via weighted least-squares fit.

Table 1. Median time, displacement, and uncertainty estimates from HTF analysis of anomalies in the GPS coordinate time series.

Site	Best-fit	Displacement (mm)			One-sigma Uncertainty (mm)		
	T_0	East	North	Up	East	North	Up
ACAP	∼1996	-16.5	-20.5	46.8	3.9	2.5	12.1
ACAP	∼1998	-5.1	-18.9	47.1	2.7	1.8	8.5
CAYA	1998.19	3.4	-29.8	25.8	1.0	0.6	2.9
POSW	1998.39	9.6	-10.4	-13.2	0.3	0.4	2.6
ACAP	∼1999	-16.9	3.0	19.7	2.8	1.7	8.2
CAYA	1999.03	-4.6	-7.9	8.2	0.9	0.5	2.6
POSW	1999.20	8.4	-2.4	-10.1	0.3	0.4	2.3
ACAP	2000.05	-5.1	1.4	27.1	2.3	1.4	6.5
CAYA	2000.04	-3.0	-3.7	5.8	0.8	0.5	2.6
POSW	2000.34	6.9	-2.0	-16.8	0.3	0.4	2.4
YAIG	∼2000	5.0	-1.8	3.2	1.2	0.7	3.6
ZIHP	∼2000	3.6	-19.8	-1.1	3.9	2.7	15.2
ACAP	2001.19	-4.1	0.2	21.2	0.9	0.7	2.9
CAYA	2000.86	2.7	-7.3	19.9	0.8	0.5	2.6
IGUA	∼2001	5.1	4.7	5.7	1.4	0.9	4.3
PINO	2001.04	-7.0	-11.4	21.3	1.3	1.0	4.4
POSW	2001.16	6.1	0.6	-3.3	0.3	0.4	2.3
YAIG	2001.06	3.7	-0.1	34.2	0.9	0.5	2.6
ZIHP	2001.27	-3.7	-6.2	9.5	1.2	0.9	4.0
ACAP	2002.15	-14.3	-42.9	37.3	0.8	0.6	2.5
CAYA	2002.16	-29.0	-61.1	71.1	1.0	0.6	3.0
IGUA	2002.17	-10.5	-36.7	-15.5	0.9	0.6	3.0
OAXA	∼2002	-10.8	-11.9	-1.4	1.3	1.0	4.3
PINO	2002.34	-13.5	-28.6	17.6	1.0	0.7	3.1
POSW	2002.20	1.9	-12.7	-12.7	0.4	0.4	2.4
YAIG	2002.18	-8.3	-20.0	17.4	1.0	0.6	3.0
ZIHP	2002.26	-13.9	-24.7	10.9	1.0	0.8	3.4
ACAP	2002.91	-6.2	-9.5	19.9	0.8	0.6	2.5
CAYA	2003.00	-4.8	-16.5	-5.3	0.8	0.5	2.6

Table 1—Continued

Site	Best-fit	Displacement (mm)			One-sigma Uncertainty (mm)		
	T_0	East	North	Up	East	North	Up
PINO	2002.96	-3.4	-11.2	9.0	0.9	0.7	2.8
POSW	∼2003	-0.6	-1.7	-9.4	0.8	0.7	4.6
YAIG	2003.04	0.9	-5.8	24.7	0.9	0.5	2.6
ZIHP	2003.05	-23.1	-29.1	19.6	1.3	0.9	4.1
ACAP	2004.06	-1.7	-3.8	23.2	0.9	0.6	2.9
CAYA	2004.15	5.6	-8.1	12.6	1.1	0.7	3.5
COYU	2004.10	1.9	-6.1	32.0	1.2	0.8	3.8
DOAR	2004.16	5.8	-6.4	11.9	1.1	0.7	3.4
IGUA	∼2004	5.0	2.0	6.9	1.1	0.7	3.6
OAXA	∼2004	-2.9	-15.4	2.1	1.6	1.1	5.0
PINO	2004.09	-4.1	-11.7	12.9	1.0	0.7	3.2
YAIG	2004.17	7.3	-1.8	36.5	0.9	0.5	2.7
ZIHP	∼2004	6.4	-14.6	15.2	1.6	1.1	5.2

Table 2. Median time, duration, and magnitude equivalent of moment release during slow slip events. Magnitude is calculated using $M_w = 3[\log_{10}(M_0) - 9.05]/2$, in which moment $M_0 = \mu \oint S \, \mathrm{d}A$, $\mu = 2 \times 10^{10}$ is shear rigidity, and S is anomalous slip. Timing parameters are the best-fit from the discretized model.

Event	Median	Timescale	Single Patch Model			Discretized Model	
	Time T_0	τ (mos)	Best-Fit M_w	95% Min	95% Max	Best-Fit M_w	Min M_w
1996	??	??	7.30	6.73	8.46	6.97	6.72
1998	1998.18	2.5	7.44	7.18	8.05	6.86	6.76
1999	1999.02	2.6	6.99	6.74	7.41	6.38	6.34
2000	2000.05	2.6	6.35	5.15	7.98	6.38	6.40
2001	2000.92	2.6	7.70	6.36	7.75	6.42	6.29
2002	2002.17	2.0	7.52	7.46	7.56	6.89	6.83
2003	2002.91	2.6	7.15	6.92	7.20	6.67	6.65
2004	2004.13	2.2	6.80	6.24	6.88	6.62	6.35